Semiclassical dynamics of a bound system in a high-frequency field

1995 J. Phys. A: Math. Gen. 28 5973

(http://iopscience.iop.org/0305-4470/28/21/008)

J. Phys. A: Math. Gen. 28 (1995) 5973–6011. Printed in the UK

Semiclassical dynamics of a bound system in a high-frequency field

Naama Brenner and Shmuel Fishman†
Department of Physics, Technion, Haifa 32000, Israel

Received 5 May 1995

Abstract. The quantal behaviour of a particle in a one-dimensional triangular potential well, driven by a monochromatic electric field, is studied. A classical high-frequency expansion together with semiclassical uniform methods are used to obtain an explicit form of the Floquet evolution operator in the unperturbed basis. A local exact solution is found for the eigenvalue equation of this operator under certain conditions. The local solution provides a tool for the quantitative investigation of the eigenstates. It predicts the appearance of quasi-resonances, or photonic states, and gives their location, shape and width as a function of parameters. It also predicts a local crossover from a decaying region to a more extended region as a function of n, with a point of crossover n_c between them. The results concerning the local structures are used to justify and extend a previously suggested method for the investigation of the asymptotic properties of the eigenstates. These are found to decay with a power depending on the field parameters (first proposed by Benvenuto *et al*). The specific system studied here is suggested as a prototype model for a class of driven one-dimensional bound systems, whose main characteristic is an increasing density of states as a function of energy.

1. Introduction

The quantum mechanical behaviour of one-dimensional systems that are chaotic in the classical limit has been studied extensively [1–6]. These systems are of conceptual interest in the field of 'quantum chaos' [1, 2, 7, 8], and are of experimental relevance as models of realistic systems [3, 9–11]. Having only one degree of freedom, these systems are easy to understand theoretically and to simulate numerically. Yet, in general, their classical dynamics is chaotic, showing complex behaviour and diffusive motion in phase space. The physical relevance of these model systems results from the fact that in many cases the motion of small driven three-dimensional objects can be described approximately by one effective degree of freedom. Such is the case, for example, for the linear molecule [9] and for the highly excited hydrogen atom in a microwave field [3]. Of particular importance in this respect is the family of models describing periodically driven one-dimensional systems, which are related to small quantum systems in periodic driving fields. For these, quantum mechanics is described in terms of the Floquet operator, which is the unitary operator of time evolution for one period [2, 12, 13].

The most well understood model system is the kicked rotor, described the Hamiltonian [4, 14, 15]

$$\mathcal{H}(\theta, p; t) = \frac{p^2}{2} + K\cos\theta \sum_{m=-\infty}^{\infty} \delta(t - m) \tag{1.1}$$

† Member of the Minerva Centre for the Nonlinear Physics of Complex Systems.

0305-4470/95/215973+39$19.50

where θ is an angle and p is the conjugate angular momentum. It describes the motion of a rigid planar rotator with a moment of inertia equal to unity and an electric dipole, in the presence of a periodic electric field with a time dependence of a train of δ-functions. The effective strength of the driving is K, and time is measured in units so that the period is unity. A possible different interpretation of this Hamiltonian (with different boundary conditions) is that of a particle in an infinite square well potential in one dimension [16]. Classically, the kicked rotor reduces to the standard map [15], being a stroboscopic map relating the variables (θ, p) at successive time periods of the external field. For large enough values of K, the trajectories in phase space of this map are diffusive, i.e. the average momentum squared satisfies $\langle p^2 \rangle \sim t$ [14, 15]. Quantum mechanics introduces an additional parameter, namely the effective Planck constant $\hbar$. The simple δ-function time dependence in this model enables the exact calculation of the Floquet operator in the basis of the unperturbed angular momentum eigenstates $|n\rangle$. One finds that it has the form of a band matrix, with the bandwidth depending on $(K/\hbar)$, and that generically the diagonal elements are pseudorandom [6]. This is the basis for a formal mapping between this problem and that of a particle in a one-dimensional lattice with random on-site potential and a finite range of hopping interaction [6]. This is a well studied problem in solid state physics [17, 18], and it is known that Anderson localization is found in this case: all eigenstates are exponentially localized on the lattice, with a typical localization length ξ. Correspondingly, the eigenstates of the Floquet operator are exponentially localized in the $|n\rangle$ basis. This implies that the classical growth in energy of the system, related to the diffusion in phase space, is suppressed in quantum mechanics by a mechanism similar to Anderson localization [5, 6, 18]. Many results from localization theory were successfully carried over to explain the dynamics of the kicked rotor [19–23]

Inspired by these ideas, much research has been performed along similar lines for other systems. Many classical systems can be approximated locally by the standard map, and therefore localization was expected to play an important role in their quantum dynamics. In particular, Casati *et al* [3] described classically the driven one-dimensional hydrogen atom (which is a good approximation to the three-dimensional highly excited hydrogen atom), by a map on a Poincaré surface of section, called the Kepler map [24]. Rather than being stroboscopic in time, this map relates the values of the external field phase and the energy of the electron at successive passes near the nucleus. This nonlinear map is locally similar to the standard map, therefore it was argued that locally its quantum dynamics should be like that of an Anderson model, with a localization length ξ related to the parameters of the local classical map [24]. Jensen *et al* [25] used an effective local quantization of the standard map on a partial set of the unperturbed basis, consisting of quasi-resonant states which dominate the dynamics. Other approaches, not related to Anderson localization, were also suggested for the theoretical treatment of the driven hydrogen atom. In particular, Blümel *et al* [26] proposed an approximation based on the fact that in different regions of unperturbed quantum number n one part of the Hamiltonian is much larger than the other. Power-law localization of the Floquet eigenstates was found numerically, and explained semiclassically to result from the structure of the position operator $\hat{x}$ in the unperturbed basis.

Some important differences between the kicked rotor and other driven systems, in particular the hydrogen atom, should be kept in mind when making use of analogies to solid state models. First of all, there is no pseudorandom element in the unperturbed spectrum of the hydrogen atom. Whereas for the kicked rotor the structure of the unperturbed energy levels $E_n \sim n^2$ results in the diagonal elements of the Floquet operator having pseudorandom phases, for the hydrogen atom $E_n \sim -1/n^2$, for which the phases are far from being pseudorandom. In contrast, for large n the sequence of phases $E_n (\mathrm{mod}\, 2\pi)$

becomes a slowly varying function of n, that is almost constant. This property is shared by other confining potentials with a discrete spectrum. Consider a potential well in one dimension which has the form of a power law, $V(x) \sim x^{\sigma}$. For $\sigma < 2$, the energy levels become dense at high energies, i.e. the level spacing tends to zero. This means that the phases $E_n(\mathrm{mod}\, 2\pi)$ are not pseudorandom [27, 28], but are a slowly varying function of n for large n. For larger powers satisfying $\sigma > 2$, the unperturbed spectrum is not slowly varying, but it is not pseudorandom either, and other kinds of behaviour can be expected [28–30]. Only in the limit of the power going to infinity, corresponding to the infinite square well, is the spectrum pseudorandom as in the case of the rotor.

Another difference, related to the first one, is the spectrum of unperturbed frequencies corresponding to transitions between unperturbed states. The kicked rotor has one basic such frequency, and all transitions are multiples of this basic frequency. The scenario of Anderson localization described above holds for the non-resonant case, where the frequency of the driving field is not rationally related to this basic frequency of the rotor. For the resonant case, the dynamics is very different: rather than suppression of energy diffusion, resonant excitation takes place [31]. On the other hand, for systems where the unperturbed spectrum E_n is a slowly varying function of n, there are many transition frequencies, and there can be many near-resonances with the external field. This is the reason for the occurrence of 'quasi-resonances' [33] or 'photon states' [24] both in the transition amplitudes and in the eigenstates of the Floquet operator.

In order to shed some light on the quantal behaviour of periodically driven systems with an asymptotically slowly varying unperturbed spectrum, a specific system of this type will be studied in the present work. It is defined by the Hamiltonian

$$\tilde{\mathcal{H}}(\tilde{x}, \tilde{p}; \tilde{t}) = \frac{\tilde{p}^2}{2m} + q\mathcal{E}_0\tilde{x} + q\mathcal{E}\tilde{x}\cos\tilde{\Omega}\tilde{t} \qquad \tilde{x} \geqslant 0 \tag{1.2}$$

where m and q are, respectively, the mass and electric charge of the particle, and $\mathcal{E}_0$ is the strength of the constant electric field which constitutes the confining well. The condition $\tilde{x} \geqslant 0$ means that there is a perfectly reflecting wall at $\tilde{x} = 0$. The strength of the time-dependent electric field is $\mathcal{E}$, and it drives the system with an angular frequency $\tilde{\Omega}$. We suggest this system as a prototype for the family of one-dimensional models where the unperturbed spectrum E_n is a slowly varying function of n. As explained above, the hydrogen atom, as well as power-law potential wells with a power smaller than 2, fall into this category. For these systems, since the classical frequency of the unperturbed motion tends to zero at high energy, an external periodic perturbation becomes of high frequency compared to the classical frequencies in this region. If one external frequency is involved, this allows the effective separation of time scales and a formal perturbative expansion around the high-frequency limit. A small parameter can be defined, which is the ratio between the unperturbed classical frequency and the driving frequency, and its dynamics can be studied classically for short times. Since the field period is a very short time scale in the problem, a semiclassical calculation of the Floquet operator using the short-time classical solutions is expected to be very accurate. Under certain conditions, it will be shown that the slowly varying nature of the unperturbed energies can be exploited to construct a local exact solution to the semiclassical eigenvalue equation. This results from the fact that locally this equation is related to that of the kicked linear rotor, which is an exactly solvable problem [34]. The local solution can be used to investigate the properties of the quasi-energy eigenstates, including a quantitative description of the quasi-resonances, their location, shape and width, and a characterization of the typical width of the eigenstate. The results concerning the local structures can, in this case, be used to justify a previously suggested method for the

study of the asymptotics of the eigenstates [32]. This method consists of a projection of an eigenvalue equation from the n-space to the partial set of quasi-resonances; therefore, the information concerning the structure of these quasi-resonances is of importance in applying it.

It should be mentioned that a model similar to (1.2) has been studied by Shimshoni and Smilansky [35], but with a driving field in the form of δ-kicks. It turns out that the results in that case are quite different from those found for the model (1.2). The reason for this difference will become clear at a later stage.

The Hamiltonian (1.2) appears in several areas of physics. It is a model for trapped charge carriers under the surface of helium IV [36]. The charge carriers are repelled from the surface into the liquid, where the dielectric constant is larger, by their image charge. If, in addition, a constant electric field $\mathcal{E}_0$ is applied perpendicular to the surface, the total potential acting on the particle is

$$\frac{Zq^2}{\tilde{x}} + q\mathcal{E}_0\tilde{x} \tag{1.3}$$

where Z is a constant depending on the dielectric constant of the liquid, q is the particle charge and $\tilde{x}$ measures its distance from the surface. The basic features of this potential are strong repulsion near the surface, and a linear dependence on the coordinate far from the surface. Therefore, the Hamiltonian (1.2) was suggested as a simplified model for this system [35].

It is also related to the motion of electrons in a very weak magnetic field, near a surface [37]. Such electrons move along 'skipping orbits', performing only small portions of the cyclotron motion and colliding with the surface at a small angle of incidence. The degree of freedom corresponding to the motion perpendicular to the wall, can be approximately described by the binding potential in (1.2). Transitions between the unperturbed levels $E_n \sim n^{2/3}$ explain accurately the peaks in the surface impedance of materials in a weak magnetic field [38].

A simple classical interpretation of (1.2), is a massive ball bouncing on a periodically vibrating platform, under the influence of gravity. This classical model has been studied by Pustylnikov [39], who proved that there are sets of initial conditions for which diffusive trajectories in phase space are found. A classical Kepler-type map was constructed by Benvenuto *et al* [40], which accounts accurately for the classical motion. For the quantum problem, numerical simulations indicate a transition from localized to extended states as a function of the driving strength [40]. An analogy was proposed to an Anderson-type model with a variance of the random potential which varies along the lattice [32]. For this solid state model, it is known that a transition takes place between power localized (normalizable) and extended (non-normalizable) states [41]. It was argued that a similar mechanism causes the delocalization of the Floquet eigenstates in the dynamical problem.

In the present work, the method outlined earlier for systems with a slowly varying spectrum will be applied to the model system (1.2). In section 2 the classical equations of motion will be solved approximately in the high-frequency field regime, and an approximate stroboscopic mapping will be constructed. In section 3, the approximate classical trajectories will be used to calculate a semiclassical approximation for the Floquet operator in the unperturbed basis. In section 4, the local solution will be presented, and properties of the eigenstates will be deduced from it. The predictions will be tested numerically wherever possible. The conclusions will be summarized and discussed in section 5.

2. Classical dynamics

In this section the classical dynamics of the model system defined by the Hamiltonian (1.2) will be investigated. For this purpose, a perturbative approach will be employed, which is appropriate for the high-frequency field regime. A small parameter will be defined, which effectively separates two time scales in the system: one (fast) related to the external field, and the other (slow) related to the unperturbed motion. The Hamiltonian (1.2) can be scaled to convenient units, so that classically it depends on two parameters: the external driving frequency and the external driving strength. A convenient transformation that is used in the present paper is $x = c_x\tilde{x}$ and $p = c_p\tilde{p}$, with $c_x = q\mathcal{E}_0$ and $c_p = 3\pi/\sqrt{m}$. The time and the frequency in these units are $t = c_x c_p \tilde{t}$ and $\Omega = \tilde{\Omega}/c_x c_p$. The value of the energy is not altered by this transformation, namely $\mathcal{H} = \tilde{\mathcal{H}}$, and it has the form

$$\mathcal{H} = \frac{p^2}{2(3\pi)^2} + x + kx\cos\Omega t \tag{2.1}$$

where $k = \mathcal{E}/\mathcal{E}_0$. Note that this transformation leads to the transformation of the value of Planck's constant, $\hbar = c_x c_p \tilde{\hbar}$, where $\tilde{\hbar}$ is Planck's constant in the units of (1.2), while $\hbar$ is its value in the units of (2.1).

The unperturbed system, described by the Hamiltonian

$$\mathcal{H}_0 = \frac{p^2}{2(3\pi)^2} + x \tag{2.2}$$

is an integrable one, with action-angle variables defined by the following energy-dependent canonical transformation:

$$I = \frac{1}{2\pi}\oint p\,\mathrm{d}x = (2E)^{3/2} \tag{2.3}$$

$$\theta = \pi \mp \pi\sqrt{1 - x/E} \tag{2.4}$$

where the (−) sign corresponds to positive momentum and (+) to negative momentum. Here the angle is defined such that it is zero when $x = 0$, at the beginning of the classical orbit, and is 2π when $x = 0$ again at the end of the orbit.

In what follows, the dynamics of the driven system will be described in terms of these variables. The full time-dependent Hamiltonian in these action-angle variables is

$$\mathcal{H}(I, \theta; t) = \frac{1}{2}I^{2/3} + \frac{k}{2\pi^2}I^{2/3}a(\theta)\cos\Omega t \tag{2.5}$$

where $a(\theta) = 2\pi\tilde{\theta} - \tilde{\theta}^2$, and $\tilde{\theta} = \theta \bmod 2\pi$. Hamilton's equations of motion are then

$$\dot{I} = \frac{k}{\pi^2}I^{2/3}(\tilde{\theta} - \pi)\cos\Omega t \tag{2.6}$$

$$\dot{\theta} = \frac{1}{3I^{1/3}} + \frac{k}{3\pi^2 I^{1/3}}a(\theta)\cos\Omega t\,. \tag{2.7}$$

These equations, of course, cannot be solved exactly for long times, since the system is chaotic. For short times, a perturbative method can be used. Rather than treating k as the small parameter and the driving field as a perturbation to the particle in the well, we take a somewhat different approach. Since the system is also integrable in the absence of the reflecting wall, we effectively take as our 'unperturbed' situation the one where the particle does not interact with the wall during most periods of the driving field. This condition is approached as the energy of the system $\mathcal{H}_0$ becomes higher, since the time of return to the

wall grows with the energy. The dimensionless parameter which controls this approximation is the ratio between the classical frequency and the field frequency,

$$\epsilon = \frac{\omega_0(I)}{\Omega} = \frac{1}{3\Omega I^{1/3}} \tag{2.8}$$

where $\epsilon = 0$ corresponds to the 'far-wall limit' [35], and our aim is to expand the solution for small but finite ϵ. To do this, it is convenient to define a dimensionless time variable

$$\tau = \Omega t \tag{2.9}$$

so that the driving field has a cycle of length 2π, namely an angular frequency of unity. To make this a canonical transformation, we accompany it by a change of the energy scale, $\mathcal{H} \to \mathcal{H}/\Omega$. We note that ϵ, being a function of the action I, varies with time. We therefore write the equations of motion for the two variables ϵ and θ as

$$\frac{\mathrm{d}\epsilon}{\mathrm{d}\tau} = \frac{k}{\pi^2}\epsilon^2(\pi - \tilde{\theta})\cos\tau \tag{2.10}$$

$$\frac{\mathrm{d}\theta}{\mathrm{d}\tau} = \epsilon + \frac{k}{\pi^2}\epsilon a(\theta)\cos\tau\,. \tag{2.11}$$

It is seen that under the assumption that $\epsilon \ll 1$, the time variation of ϵ is slower than that of θ. Therefore, it is possible to solve the equation via an iterative process of a Born–Oppenheimer type. In what follows, we will always measure the time from the beginning of a cycle of the electric field. Similar formulae, but more complicated, can be derived for the more general case where the initial time is $\tau_0 \neq 0$.

The first step is to assume that ϵ is constant, and to solve the equation for θ. This is the first order in ϵ, and one obtains

$$\theta(\tau) = \theta_0 + \epsilon_0\tau + \epsilon_0\frac{k}{\pi^2}a(\theta_0)\sin\tau \tag{2.12}$$

where $\theta_0 = \theta(\tau = 0)$ and $\epsilon_0 = \epsilon(\tau = 0)$. To lowest order the motion in θ is linear in time (with the coefficient ϵ_0), with oscillations of unit frequency on top of the smooth motion. The magnitude of the oscillations depends on θ_0 as well as on ϵ_0, being maximal at $\theta_0 = \pi$ and approaching zero as θ_0 approaches the ends of the interval $[0, 2\pi]$.

The next step is to insert the solution for $\theta(\tau)$ into the equation for ϵ and solve it to second order in ϵ_0. It should be noted that the equation of motion for ϵ, equation (2.10), includes a mod operation. In general this introduces great complexity into the solutions, but since we are interested in solutions only for short times, there will be at most one 'jump' mod 2π of $\theta(\tau)$ within a period of the external field. This is because of our assumption that $\epsilon \ll 1$, which implies that during the field cycle the particle completes only a small fraction of the unperturbed period, corresponding to the angle θ completing only a small fraction of a cycle of 2π. According to the definition of θ, it equals an integer multiple of 2π whenever the coordinate x is zero, i.e. when the particle collides with the wall. Therefore the 'jump' mod 2π is exactly the collision with the wall, and under our assumptions it can occur at most once during the external field period. The two cases of a cycle with and without a collision will yield two different solutions for $\epsilon(\tau)$. It is helpful to define the 'collision time' τ^* by the equation $\theta(\tau^*) = 2\pi$. A collision will occur in a cycle, only if the angle θ_0 at the beginning of the cycle is close enough to 2π, so that $\tau^* < 2\pi$. In this region of initial conditions, the function $a(\theta_0)$ is small, so that τ^* is determined to first order by the equation

$$\theta_0 + \epsilon\tau^* = 2\pi\,. \tag{2.13}$$

This may be formulated as a condition on θ for the occurrence of a collision in the cycle, namely for $\tau^* < 2\pi$:

$$\theta_0 > \theta^* = 2\pi(1-\epsilon)\,. \tag{2.14}$$

It can now be checked that indeed $a(\theta_0)$ is $\mathcal{O}(\epsilon)$ in this region, so that it is consistent to neglect it in the first-order approximation for τ^*. The solution for $\epsilon(\tau)$ can now be written, with the two cases—collision or no collision—determined by the initial angle. If $\theta_0 < \theta^*$, i.e. the initial condition at the beginning of the cycle is such that no collision will occur, one obtains

$$\epsilon(\tau) = \epsilon_0 - \epsilon_0^2\frac{k}{\pi^2}(\theta_0-\pi)\sin\tau - \epsilon_0^3\frac{k}{\pi^2}g(\tau) - \epsilon_0^3\frac{k^2}{2\pi^4}\left[a(\theta_0) - 2(\theta_0-\pi)^2\right]\sin^2\tau \tag{2.15}$$

where $g(\tau) = (\tau\sin\tau + \cos\tau - 1)$. In this case $\epsilon(\tau)$ changes periodically within the cycle, leaving no net change at the end:

$$\epsilon(2\pi) = \epsilon_0\,. \tag{2.16}$$

If, on the other hand, $\theta_0 > \theta^*$, i.e. the initial angle is sufficiently close to 2π for a collision to occur, one finds

$$\epsilon(\tau) = \epsilon_0 - \epsilon_0^2\frac{k}{\pi^2}f(\tau,\theta_0) - \epsilon_0^3\frac{k}{\pi^2}g(\tau) + \frac{k^2}{\pi^4}\epsilon_0^3[f(\tau,\theta_0)]^2 \tag{2.17}$$

where

$$f(\tau,\theta_0) = \begin{cases} (\theta_0-\pi)\sin\tau & \tau < \tau* \\ \left[(\theta_0-3\pi)\sin\tau + 2\pi\sin\tau^*\right] & \tau > \tau*\,. \end{cases} \tag{2.18}$$

In this case there is a net change in $\epsilon(\tau)$ over one field period. With the help of (2.8), the solution can now be written to the order of ϵ_0^3 in terms of the canonical variable I: for a cycle with no collision, one finds

$$I(\tau) = I_0 + \frac{k}{\Omega\pi^2}(\theta_0-\pi)I_0^{2/3}\sin\tau + \frac{k}{3\Omega^2\pi^2}I_0^{1/3}g(\tau) + \frac{k^2}{6\pi^4\Omega^2}\left[a(\theta_0) + 2(\theta_0-\pi)^2\right]I_0^{1/3}\sin^2\tau \tag{2.19}$$

while for a cycle with a collision,

$$I(\tau) = I_0 + \frac{k}{\pi^2\Omega}I_0^{2/3}f(\tau,\theta_0) + \frac{k}{3\pi^2\Omega^2}I_0^{1/3}g(\tau) + \frac{k^2}{3\Omega^2\pi^4}I_0^{1/3}[f(\tau,\theta_0)]^2\,. \tag{2.20}$$

In figure 1, the solution for $I(\tau)$ to second order in ϵ is shown, within a cycle that contains a collision. The function $I(\tau)$ has a cusp at $\tau = \tau^*$, the collision time. The perturbative solution (squares) is compared to the exact numerical integration of (2.6) and (2.7).

The relation between the values of θ and I at a fixed time in successive cycles of the electric field, defines a classical mapping. This may be written, to first order in ϵ_0, as

$$I_{n+1} = \begin{cases} I_n & \theta_n < \theta^* \\ I_n + \dfrac{2k}{\pi\Omega}I_n^{2/3}\sin\tau^* + \dfrac{4k^2}{3\Omega^2\pi^2}I_n^{1/3}\sin^2\tau^* & \theta_n > \theta^* \end{cases} \tag{2.21}$$

$$\theta_{n+1} = \theta_n + \frac{2\pi}{3\Omega}I_n^{-1/3}$$

where I_n and θ_n are the values of the dynamical variables at the beginning of the nth field cycle. The two branches of I_{n+1} correspond to θ_n being less than or greater than θ^*, i.e. to the occurrence or absence of a collision.

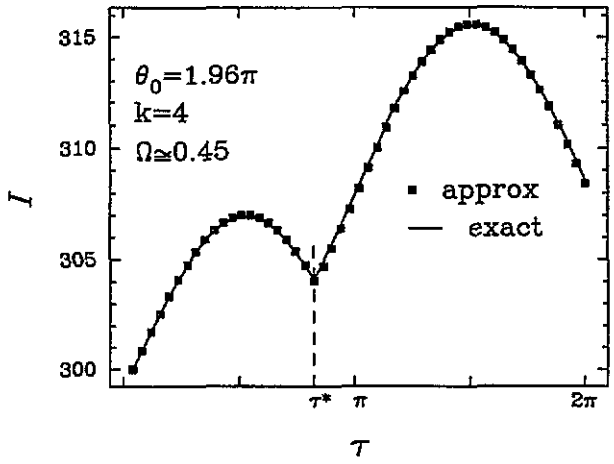

Figure 1. The perturbative solution (squares) for the action variable $I(\tau)$ within one field cycle containing a collision, compared to the exact numerical solution (full curve). The collision time is τ^*.

In principle, the method described above allows one to proceed to higher orders in ϵ_0. The solution for $\theta(\tau)$ to second order in ϵ_0 is presented in appendix A as an example, where the time variation $\epsilon(\tau)$ is taken into account. This is the next step in the iterative Born–Oppenheimer procedure. It should be noted that τ^* and θ^*, being dependent on both dynamical variables, must also be expanded in powers of ϵ_0 to the correct order. The calculation of the Jacobian of the map (2.21) to first order, given in appendix B, demonstrates this expansion. It is seen that in order to include all first-order terms in the Jacobian, the map should be calculated to a higher order.

A qualitative picture of the dynamics may be described from the lowest order in (2.21). In this approximation, for some initial conditions there is free dynamics, whereas for the others, the particle undergoes a collision with the wall, which, similar to a 'kick', may change its action. Therefore the field effectively transfers energy to the particle only near the wall, whereas far away from the wall its effect reduces to local oscillations of the action with no net change. Previous works [40] have exploited this fact to construct an 'impact mapping' relating the action before and after a collision. As I becomes larger, the time between collisions becomes longer, and the motion is regular for longer periods of time. The effectiveness of the 'kick', however, also grows with I, so that looking at long times compared to the classical period the motion is never really regular. This qualitative picture allows one to calculate the average rate of diffusion in I. Each time the particle collides with the wall, it acquires an additional action

$$\Delta I \approx \frac{2k}{\pi\Omega} I^{2/3} \sin\tau^* . \tag{2.22}$$

Assuming τ^* to be uncorrelated at different collisions, this averages over many collisions to

$$\langle \Delta I^2 \rangle \approx \frac{2k^2}{\pi^2\Omega^2} I^{4/3} . \tag{2.23}$$

The time between collisions is approximately equal to the unperturbed cycle time, $T = 6\pi I^{1/3}$, so that as a function of the time τ

$$\langle \Delta I^2 \rangle \approx \frac{k^2}{3\pi^3 \Omega^3} I \tau \,. \tag{2.24}$$

This is the same result as obtained by the impact mapping [40], but in different variables.

In order to describe a global picture of the phase space under the action of the map (2.21), it is helpful to find some of the periodic orbits, or fixed points of order r, of the map. These are defined by the equations

$$I_{n+r} = I_n \qquad \theta_{n+r} = \theta_n + 2\pi l \tag{2.25}$$

where l is the winding number, resulting from the periodicity of phase space in θ. The fixed points of lowest order r are easily found assuming that the particle hits the wall at most once during the period of the fixed point. If this is the case, the action changes only at one field cycle of the period, whereas it stays constant in all other field cycles. Solving the equation for θ in (2.25) and (2.21), it is seen that to the leading order the values of I at the fixed points satisfy

$$\frac{\omega_0(I)}{\Omega} = \frac{l}{r} \,. \tag{2.26}$$

This is simply the resonance condition. Since $\omega_0(I)/\Omega = \epsilon$, only orbits with $l/r \ll 1$ can be found in the framework of our approximation. Equation (2.26) can be written as a condition on I,

$$I^{(r,l)} = \left(\frac{r}{3\Omega l}\right)^3 \,. \tag{2.27}$$

It is seen that for a given r there is a maximal value of I (corresponding to $l = 1$), where a period of length r occurs; at larger actions, only fixed points of higher order are found. From the equations for I in (2.25) and in (2.21), one finds that the fixed points must also satisfy $\sin \tau^* = 0$. For each given I, this is a condition on the angle θ. There are two types of fixed points, determined by the value of $\cos \tau^*$. For the first kind, where $\cos \tau^* = 1$, one finds that $\theta_j = 2\pi l j / r$, where $1 \leqslant j \leqslant r$. This means that θ passes through the two endpoints of the segment $[\theta^*, 2\pi]$, which is the segment of initial conditions for which collisions occur. At these endpoints, $\tau^* = 0$ or 2π and the action remains unchanged, therefore these are fixed points. The stability of the periodic orbit is found by diagonalization of the local monodromy matrix to leading order. For the case $\cos \tau^* = 1$, it is found that the fixed points are unstable, and denoting the eigenvalues by $e^{\pm u_p}$, one finds

$$u_p = \left(4k\frac{l}{r}\right)^{1/2} = \mathcal{O}(\sqrt{k\epsilon}) \,. \tag{2.28}$$

Thus the mapping becomes less unstable for large values of I. The second kind of periodic orbit is found for $\cos \tau^* = -1$. These also occur at actions I satisfying (2.27), and are composed of the points $\theta_j = \pi l(2j+1)/r$, where $0 \leqslant j \leqslant (r-1)$. This orbit passes through the middle of the segment $[\theta^*, 2\pi]$, where $\tau^* = \pi$. These fixed points are stable, and the eigenvalues of the monodromy matrix are $e^{\pm i u_p}$. The two periodic orbits at the same value of I form a chain of alternating stable and unstable fixed points.

A typical set of phase-space trajectories of the approximate map (2.21) is shown in figure 2(a). The trajectories are shown only in the vicinity of the unstable fixed points, since near the stable ones the violation of area preservation in the approximate map makes long trajectories meaningless. Figure 2(b) shows a set of trajectories of the exact mapping, obtained by numerical integration of (2.6) and (2.7). For the sake of comparison,

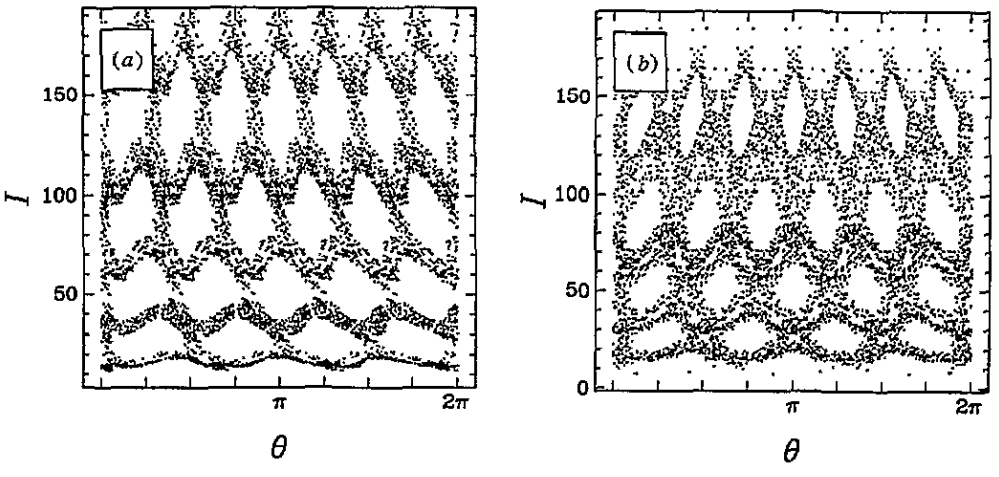

Figure 2. Phase-space trajectories in the vicinity of the unstable periodic orbits, for $k = 0.5$ and $\Omega \simeq 0.45$. (*a*) The approximate map, (*b*) the exact map.

only trajectories near the unstable fixed points are shown for the exact mapping as well. The general structure of the fixed points can still be seen clearly from this partial set of trajectories.

It should be noted, in concluding this section, that the procedure presented above can be applied to other situations. Consider a Hamiltonian in action angle variables,

$$\mathcal{H}_0(I,\theta;t) = \mathcal{H}_0(I) + kV(I)a(\theta)f(t) \tag{2.29}$$

where $\mathcal{H}_0(I) = AI^\alpha$ and $V(I) = BI^\beta$, with positive α and β, while $a(\theta)$ is a 2π periodic function, and $f(t)$ is periodic in time with a frequency Ω. If $0 < \alpha < 1$, the small parameter $\epsilon = \alpha A I^{\alpha-1}/\Omega$ can be defined, and equations of motion for θ and for ϵ take the form

$$\frac{\mathrm{d}\epsilon}{\mathrm{d}\tau} = F_1(k,\Omega,\theta)\epsilon^{\frac{\alpha+\beta-2}{\alpha-1}} f(\tau) \tag{2.30}$$

$$\frac{\mathrm{d}\theta}{\mathrm{d}\tau} = \epsilon + F_2(k,\Omega)\epsilon^{\frac{\beta-1}{\alpha-1}} f(\tau) \tag{2.31}$$

where

$$F_1 = \frac{(1-\alpha)Bk\Omega^{\frac{\beta-\alpha}{\alpha-1}}}{(A\alpha)^{\frac{\beta-\alpha}{\alpha-1}}}\frac{\mathrm{d}a}{\mathrm{d}\theta} \tag{2.32}$$

and

$$F_2 = \frac{kB\beta\Omega^{\frac{\beta-\alpha}{\alpha-1}}}{(A\alpha)^{\left(\frac{\beta-1}{\alpha-1}\right)}}. \tag{2.33}$$

If $\beta < \alpha$, the time dependence of θ is dominated, to lowest order, by the unperturbed motion, and is faster than the time variation of I. Then, a Born–Oppenheimer-type expansion similar to the one applied here, can be used to find the approximate classical solutions for one cycle of the external driving.

3. Semiclassical dynamics

In this section the quantum dynamics of the system will be analysed in the framework of the semiclassical approximation, taking as the classical input the approximate results of the

previous section. A form of the semiclassical approximation for Feynman's path integral will be used to calculate the evolution operator for one cycle of the electric field. The units used in this section are the same as in the previous one, namely those of the Hamiltonian (2.1) scaled by $1/\Omega$, with the dimensionless time τ.

The semiclassical propagator in the action representation is [42]

$$K(I', \tau'; I, \tau) = \sum_j A_j(I', I) \exp \frac{\mathrm{i}}{\hbar} \{S_j(I', I)\} \tag{3.1}$$

where the sum is over classical trajectories connecting I at time τ to I' at time τ'. The action $S_j(I', I)$ is the generating function of the canonical transformation of time evolution along this classical trajectory:

$$S_j(I', I) = \int_\tau^{\tau'} \mathrm{d}u \{-\theta(u)\dot{I}(u) - \mathcal{H}[I(u), \theta(u)]\} \tag{3.2}$$

where $I(u)$ and $\theta(u)$ are the dynamical variables along the jth trajectory. The amplitudes $A_j(I', I)$ are related to this classical generating function via

$$A(I', I) = \left[-\frac{1}{2\pi \mathrm{i}\hbar} \frac{\partial^2 S_j(I', I)}{\partial I' \partial I} \right]^{1/2} . \tag{3.3}$$

One must therefore solve the classical 'boundary-value problem': given two endpoints I and I', find the classical paths connecting them in a given time, and calculate the corresponding generating function S. In our case, we are interested in time evolution over one period of the external field, i.e. $\tau' - \tau = 2\pi$. The time is measured, as usual, so that a cycle begins at $\tau = 0$; this restriction is only for convenience and is not an essential one. If the action is I at time $\tau = 0$, then to leading order the action at time $\tau = 2\pi$ is

$$I(2\pi) = \begin{cases} I & \theta < \theta^* \\ I + \dfrac{2k}{\pi\Omega} I^{2/3} \sin \tau^* & \theta > \theta^* \end{cases} \tag{3.4}$$

where here θ is the angle at the beginning of the cycle (which was denoted by θ_0 in the previous section), and τ^* is the time of collision with the wall. To the leading order, $\tau^* = (2\pi - \theta)/\epsilon$, where $\epsilon = \omega_0(I)/\Omega$. Consider first the case of the boundary value problem with $I' \neq I$, corresponding to the off-diagonal transition amplitudes. In this case, the classical path must be such that

$$I' = I + \frac{2k}{\pi\Omega} I^{2/3} \sin \tau^* . \tag{3.5}$$

For a given pair (I, I'), the classical paths are determined by the initial value of θ. Expressing τ^* as an explicit function of I and θ, we find the equation for this initial coordinate

$$\theta = 2\pi - \epsilon \arcsin \left(\frac{\pi\Omega}{2k} \frac{(I' - I)}{I^{2/3}} \right) . \tag{3.6}$$

If the argument of the arcsin is of absolute value less than one, there are two distinct real values θ satisfying (3.6). In this case, I and I' satisfy the following condition:

$$|I' - I| \leqslant \frac{2k}{\pi\Omega} I^{2/3} . \tag{3.7}$$

These two values of θ correspond to the two branches of the arcsin. They are the initial conditions of two distinct classical paths satisfying the boundary conditions. The two solutions coalesce when an equality holds in (3.7). This is the limit of the classically allowed

region, and beyond it only complex values of θ satisfy (3.6). The regular semiclassical approximation breaks down in what is known as a catastrophe, when such a coalescence of classical paths occurs. Rather than treating each region separately, it is possible to use a uniform approximation to get an expression which is valid on both sides of the singular point, as well as near it. This approximation consists of making a coordinate transformation which leaves unchanged the structure of stationary points of the path integral, i.e. their number, position, and the second variation in their vicinity. Therefore, the semiclassical approximation remains unchanged. This method is applicable for ordinary integrals [43] as well as path integrals [44]. The situation where only two classical paths coalesce is the simplest case of a catastrophe. A cubic transformation gives the integral in terms of Airy functions and their derivatives; this is the well known Airy approximation [45]. An alternative transformation to a cosine function is more suitable for finite integrals with periodic boundary conditions. This gives the integral in terms of Bessel functions and their derivatives [46].

It is convenient to use the uniform approximation in the 'initial-value representation' [44]. This method will be used in this section. The expression for the propagator (3.1) can be derived as a stationary phase approximation of a path integral, where the sum over classical paths is a sum over the stationary points. The initial-value representation expresses this path integral as a regular integral over the initial conditions θ, of a function which has a similar stationary point structure, and in particular has the same type of catastrophe or coalescence of stationary points. Within the semiclassical (stationary phase) approximation, the initial-value representation of the propagator is equivalent to (3.1), and it is only in this sense that the corresponding integral should be understood. The initial variables of a classical trajectory at time τ will be denoted by (I, θ), while the final values of the variables on the same trajectory at time τ' will be denoted by (I^f, θ^f). These values depend on the initial values (I, θ) through the equations of motion. In this notation, the transition amplitude takes the form [44]

$$K(I', \tau'; I, \tau) \approx \frac{1}{2\pi\hbar} \int_0^{2\pi} \left(\frac{\partial \theta^f(\theta)}{\partial \theta} \right)^{1/2} e^{\frac{i}{\hbar} F(\theta)} \, d\theta \tag{3.8}$$

where

$$F(\theta) = S(I^f(\theta), I) + [I^f(\theta) - I']\theta^f(\theta) . \tag{3.9}$$

This representation holds if the condition

$$\frac{\partial \theta^f(\theta)}{\partial \theta} \neq 0 \tag{3.10}$$

is satisfied for all values of θ [44].

In what follows, we will use the approximate solutions of the classical equations of motion, obtained in the previous section, to calculate approximate expressions for the action $S(I', I)$ and the transition amplitudes $K(I', 2\pi; I, 0)$. We would like to point out that this procedure is perturbative in the small parameter ϵ defined in section 1, and not in the strength of the driving field. In particular, for every value of the external field, there exists a region where the quantum number $n = I/\hbar$ is sufficiently large so that this approximation holds.

We will use an approximation to $S(I', I)$ that contains the two terms leading in ϵ, which are of order ϵ^{-2} and ϵ^{-1}. To get all the terms of this order, one needs to take into account only the first-order solution for $\theta(\tau)$, and two orders in the solution for $I(\tau)$: those proportional to $I^{2/3}$ and to $I^{1/3}$. One should also take into account the fact that the propagator is large only in the region of allowed classical paths, and therefore $|I - I'|$ is

effectively of order $I^{2/3}$, as is clear from (3.7). Note that to the off-diagonal elements, only cycles which contain a collision contribute. The solutions to this order, given by (2.12), (2.19) and (2.20), are substituted into (3.2). The integral over the cycle is performed in two parts, before the collision ($\tau < \tau^*$) and after it ($\tau > \tau^*$), with the corresponding parts of the solutions used in each part. The result is

$$S(I', I) \approx -2\pi\mathcal{H}_0(I) - \frac{4k}{\Omega} I^{2/3} \sin\tau^* + \frac{2k}{3\pi\Omega^2} I^{1/3} g(\tau^*) \\ -\frac{4k}{3\Omega^2} I^{1/3} \sin\tau^* + \frac{4k^2}{3\pi^3\Omega^2} \theta(\theta - 3\pi) I^{1/3} \sin^2\tau^* . \tag{3.11}$$

Using the map (2.21) for the expression of (I, θ) at the end of the cycle in terms of the values at the beginning of the cycle, one finds

$$F(\theta) \approx -2\pi\mathcal{H}_0(I) + 2\pi\epsilon(I - I') + \theta(I - I') + R(\cos\tau^*(\theta) - 1) \tag{3.12}$$

where $R = (2k/3\pi\Omega^2)I^{1/3}$. Equation (2.21) implies that $(\partial\theta^f/\partial\theta) = 1$. The transition amplitude is thus, according to (3.8),

$$K(I', 2\pi; I, 0) = \mathrm{e}^{\frac{i}{\hbar}\Phi(I, I')}\mathcal{I} \tag{3.13}$$

where the phase Φ is defined by

$$\Phi(I, I') = -2\pi\mathcal{H}_0(I) + 2\pi\left(\epsilon + \tfrac{1}{2}\right)(I - I') - R \tag{3.14}$$

and $\mathcal{I}$ is the integral

$$\mathcal{I} = \frac{1}{2\pi\hbar} \int_{-\pi}^{\pi} \exp\frac{i}{\hbar}\{(I - I')\theta + R\cos\tau^*(\theta + \pi)\}\,\mathrm{d}\theta . \tag{3.15}$$

If there is no collision, $F(\theta)$ takes the value found for $\tau^* = 0$ (or 2π), as can be verified by direct calculation. Therefore, the function $\tau^*(\theta)$ has been extended to be zero in the region of no collision, $\theta < \theta^*$. The dependence of R, ϵ and τ^* on I has been suppressed for convenience of notation. The integral of (3.8) has been transformed to the region $[-\pi, \pi]$. It is now in a form suitable for the non-integer Bessel uniform approximation as presented in [46]. The integral representation of the Bessel function used is

$$J_\nu(\zeta) = \frac{i^\nu}{2\pi} \int_{-\pi-i\infty}^{\pi-i\infty} \mathrm{e}^{-i(\zeta\cos\theta + \nu\theta)}\,\mathrm{d}\theta . \tag{3.16}$$

Denoting the phase of the integrand in (3.15) by $G(\theta)/\hbar$, the Bessel approximation is obtained by the following transformation:

$$\frac{1}{\hbar}G(\theta) = -\zeta\cos y - \nu y + A \tag{3.17}$$

where ζ, ν and A are real parameters to be determined. The parameters of the transformation are found, as usual in uniform approximations, by identification of the stationary points and by the expansion of the Jacobian in their vicinity. However, in the non-integer Bessel approximation an arbitrariness remains since there are three unknowns. It is known that for all possible solutions, this approximation reduces asymptotically to the Airy approximation [46]. In our case, a simple solution is naturally chosen, since for the special case $\epsilon = 1$ the integral (3.15) is proportional to a Bessel function. It will be assumed first that $I' > I$ and that the stationary points are real.

Assuming that ζ and ν are positive, one finds the following equations from the requirement that the transformation $\theta \to y$ maps stationary points onto stationary points:

$$\begin{aligned}\frac{1}{2\hbar}(G_1+G_2) &= A-\frac{\pi}{2}\nu \\ \frac{1}{2\hbar}(G_2-G_1) &= \sqrt{\zeta^2-\nu^2}-\nu\arccos\left(\frac{\nu}{\zeta}\right)\end{aligned} \tag{3.18}$$

where $G_{1(2)}$ denotes the value of $G(\theta)$ at the first (second) stationary point. These values satisfy

$$\begin{aligned}\frac{1}{2\hbar}(G_1+G_2) &= \frac{(I-I')}{\hbar}\pi(1-\epsilon/2) \\ \frac{1}{2\hbar}(G_2-G_1) &= \frac{1}{\hbar}\sqrt{R^2-\epsilon^2(I'-I)^2}-\frac{\epsilon}{\hbar}(I'-I)\arccos\left[\frac{\epsilon}{R}(I'-I)\right].\end{aligned} \tag{3.19}$$

Equating the two expressions, one finds the equations for the unknowns ζ, ν and A. We choose the solution

$$\begin{aligned}\zeta &= R/\hbar \\ \nu &= \epsilon(I'-I)/\hbar \\ A &= \frac{\pi}{\hbar}(I-I')-\frac{\pi\epsilon}{\hbar}(I-I').\end{aligned} \tag{3.20}$$

One may easily verify that the transformation reduces to the trivial one expected for the case $\epsilon = 1$. The next stage in the uniform approximation is to expand the Jacobian as $(\mathrm{d}\theta)/(\mathrm{d}y) \approx p_0 + q_0 \cos y$, and to demand that this expansion is identical at the stationary points. One finds that $p_0 = \epsilon$ and $q_0 = 0$. A similar procedure can be carried out for the classically forbidden region, where the stationary points are complex. The final result obtained with the help of the representation (3.16) is, for $I' > I$,

$$\mathcal{I} \approx \frac{\epsilon}{\hbar}\,\mathrm{e}^{\frac{\mathrm{i}\pi}{2\hbar}\epsilon(I'-I)-\frac{\mathrm{i}\pi}{\hbar}(I'-I)}\,J_\nu(\zeta). \tag{3.21}$$

This approximation is justified if $\zeta = R/\hbar$ is much larger than unity, which holds in the semiclassical limit $\hbar \to 0$ or $I \to \infty$. Note also that even though the two stationary points become closer to one another as $I \to \infty$, the value of the phase $G(\theta)/\hbar$ at these points remains well separated, as is easily seen from (3.19). The resulting expression for the off-diagonal transition amplitude in the semiclassical approximation is, for $I' > I$,

$$K(I', 2\pi; I, 0) = \frac{\epsilon}{\hbar}\exp\frac{\mathrm{i}}{\hbar}\left\{-2\pi\mathcal{H}_0(I)-2\pi(I'-I)-\frac{3\pi\epsilon}{2}(I'-I)-R\right\}J_\nu(\zeta). \tag{3.22}$$

By the same calculation, it is found that for $I' < I$ the transition amplitude is

$$K(I', 2\pi; I, 0) = \frac{\epsilon}{\hbar}\exp\frac{\mathrm{i}}{\hbar}\left\{-2\pi\mathcal{H}_0(I)-2\pi(I'-I)-\frac{\pi\epsilon}{2}(I'-I)-R\right\}J_{|\nu|}(\zeta). \tag{3.23}$$

We now consider the diagonal amplitudes $K(I, 2\pi; I, 0)$. In this case, there are classical paths of two kinds satisfying the boundary-value problem—paths with and without a collision with the wall. Since the semiclassical propagator is constructed as a sum over all classical paths satisfying the boundary conditions, we will consider the two types of paths separately and then add their contributions. Denoting by K_c the contribution from the paths that collide with the wall and by K_0 the contribution from those that do not collide, we write

$$K(I, 2\pi; I, 0) = K_c(I, 2\pi; I, 0) + K_0(I, 2\pi; I, 0). \tag{3.24}$$

In the region of initial angles where a collision occurs ($\theta > \theta^*$), there is an isolated initial angle θ in the middle of the interval which leaves I unchanged, corresponding to $\tau^* = \pi$. Also the two endpoints of the interval, corresponding to $\tau^* = 0$ and $\tau^* = 2\pi$, leave I unchanged. Note that these two endpoints correspond to two different values of the initial angle θ. They mark the borders between the regions with and without a collision with the wall. Application of the initial-value representation to the collision region is similar to the calculation of the off-diagonal propagator, and yields

$$K_c(I, 2\pi; I, 0) = \frac{\epsilon}{\hbar} e^{\frac{i\Phi(I,I)}{\hbar}} J_0(\zeta) \tag{3.25}$$

where J_0 is the Bessel function of zero order, and Φ is given by (3.14).

In the region where no collision occurs ($\theta < \theta^*$), there is a non-generic degeneracy of classical paths. All initial conditions in this interval result in an unchanged action over the field cycle, and must therefore contribute to the diagonal propagator. This situation is similar to the one encountered for integrable systems, where the action is conserved at all times. In this case the propagator is known to be proportional to a δ-function. A straightforward application of the semiclassical approximation (3.1) to this case is, of course, not possible since the amplitudes diverge. It can be shown, however, that the initial-value representation can capture such a singularity [44]. This is done by adding a small term $\delta\mathcal{H}_1$ to the Hamiltonian, which lifts the degeneracy between the continuum of paths. Then, it is possible to derive the form of the initial-value representation for the propagator to the leading order in δ. Taking the limit $\delta \to 0$ at the end of the calculation, gives the correct result for the semiclassical propagator corresponding to the degenerate Hamiltonian. The calculation of the propagator in the momentum representation for a free particle with a small perturbing potential, is shown as a detailed example in [44] (second paper). A similar calculation in our case yields

$$K_0(I, 2\pi; I, 0) = \frac{1}{\hbar} e^{-\frac{2\pi i}{\hbar}\mathcal{H}_0(I)}(1 - \epsilon)\,. \tag{3.26}$$

In summary, we find for the diagonal propagator the sum of the two terms,

$$K(I, 2\pi; I, 0) = \frac{1}{\hbar} e^{-\frac{2\pi i}{\hbar}\mathcal{H}_0(I)}\left[1 + \epsilon\left(J_0(\zeta)e^{-i\zeta} - 1\right)\right]. \tag{3.27}$$

The quantum action assumes the discrete values $I_n = n\hbar$, and the propagator is a discrete matrix in the $|n\rangle$ representation. Its elements are, for $n' > n$,

$$\begin{aligned}\langle n'|\hat{U}|n\rangle &= \hbar K(\hbar n', \hbar n) \\ &= e^{-\frac{2\pi i}{\hbar}\mathcal{H}_0(n\hbar)}\left\{(1-\epsilon)\delta_{n,n'} + \epsilon\, e^{-i\frac{3}{2}\pi\epsilon(n'-n)-i\zeta} J_\nu(\zeta)\right\}.\end{aligned} \tag{3.28}$$

The corresponding expression for $n' < n$ is found from (3.23). In these expressions, all I-dependent quantities which have been previously defined should be understood as calculated at $I = n\hbar$, for example $\epsilon = \epsilon(n\hbar)$, $\zeta = R(n\hbar)/\hbar$, etc. For small ϵ, the diagonal elements of the matrix have an absolute value close to unity. Neglecting the term of first order in ϵ, their phase is the free propagation exponent of the unperturbed system. As already mentioned earlier, these phases are *not* pseudorandom [28, 29].

The off-diagonal elements are first-order corrections in ϵ. Remembering the definition of $\epsilon = 1/(3\Omega(n\hbar)^{1/3})$ and using the asymptotic expansion of $J_\nu(\zeta)$, one sees that the magnitude of the off-diagonal terms decreases slowly as a function of column number, namely as $n^{-1/2}$. For a given column of the matrix, the Bessel function implies an effectively finite bandwidth b beyond which the elements decrease rapidly as a function of $|n - n'|$. The edge of the

band is where the argument and order of the Bessel function are approximately equal. This width, however, changes with the column number:

$$b(n) = \frac{4k}{\pi\Omega\hbar}(n\hbar)^{2/3}. \tag{3.29}$$

From the general structure of a row of the matrix (3.28), one may estimate the staying probability at state n after a time $\tau = 2\pi$:

$$P(n \to n) = 1 - \sum_{n' \neq n} |\langle n'|\hat{U}|n\rangle|^2 \approx 1 - \frac{2}{3\pi\Omega}(n\hbar)^{-1/3} = 1 - \frac{2}{\pi}\epsilon \approx \mathrm{e}^{-\frac{2}{\pi}\epsilon}. \tag{3.30}$$

This implies that the characteristic time for transitions (defined, for example, as the time after which $P(n \to n) = 1/\mathrm{e}$) is not the period of the electric field, but rather the unperturbed classical period, which is proportional to $1/\epsilon$. This is obvious from heuristic classical considerations, since the action is conserved for many field periods when the particle is far away from the wall. It implies, through uncertainty, that these transitions will not have a constant width in energy, but rather a width proportional to ϵ; taking into account correctly the density of states, one finds that the transitions have a width which is constant in action space.

The increasing bandwidth structure has been noticed previously in numerical calculations. In [48], the time dependence of the electric field was chosen to consist of two truncated parabolas, similar in general shape to a sine function. Exact methods known for a quadratic time dependence were used to calculate the Floquet operator numerically in the unperturbed representation. The effective bandwidth was found to fit a power-law dependence on the line number, with a power of 0.5–0.7, in agreement with the power of $\frac{2}{3}$ found in the present work.

The expression (3.29) for the bandwidth as a function of column number was obtained using first-order perturbation theory in ϵ. It marks the edge of the classically allowed region, and is therefore related to the classical equations of motion. A bound on this width, without relying on the perturbative solutions, can be obtained directly from the differential equation for $I(\tau)$:

$$\frac{\mathrm{d}I}{\mathrm{d}\tau} = \frac{k}{\pi^2\Omega} I^{2/3}(\tilde{\theta} - \pi)\cos\tau. \tag{3.31}$$

Since $\tilde{\theta} = \theta \bmod 2\pi$, one has $|\tilde{\theta} - \pi| \leqslant \pi$ and

$$\left|\frac{\mathrm{d}I}{\mathrm{d}\tau}\right| \leqslant \frac{k}{\pi\Omega} I^{2/3}. \tag{3.32}$$

The bandwidth at column n is the maximal change in the action variable after one field period, for the initial condition $I(0) = n\hbar$. In order to put a bound on $|\Delta I| = |I(2\pi) - I(0)|$, consider first the quantity $|\Delta I^{1/3}| = |I(2\pi)^{1/3} - I(0)^{1/3}|$. It satisfies

$$|\Delta I^{1/3}| = \left|\int \mathrm{d}I^{1/3}\right| = \frac{1}{3}\left|\int \frac{\mathrm{d}I}{I^{2/3}}\right| \leqslant \frac{1}{3}\int_0^{2\pi} \frac{k}{\pi\Omega}\,\mathrm{d}\tau \tag{3.33}$$

where the last inequality follows from (3.32). One finds, therefore,

$$|I(2\pi)^{1/3} - I(0)^{1/3}| \leqslant \frac{2k}{3\Omega}. \tag{3.34}$$

This can be stated as a bound on $|\Delta I|$ itself,

$$|\Delta I| \leqslant \frac{2k}{\Omega} I(0)^{2/3} \pm 3\left(\frac{2k}{3\Omega}\right)^2 I(0)^{1/3} + \left(\frac{2k}{3\Omega}\right)^3 \tag{3.35}$$

where the $\pm$ sign corresponds to the positive and negative values of ΔI, respectively. It is seen that for small ϵ, the main contribution comes from the first term, and the power $\frac{2}{3}$ of I is found. The corrections are indeed of higher order in ϵ and are proportional to $I(0)^{1/3}$. Since this is only an upper bound, the prefactors are different from those of the perturbative solution.

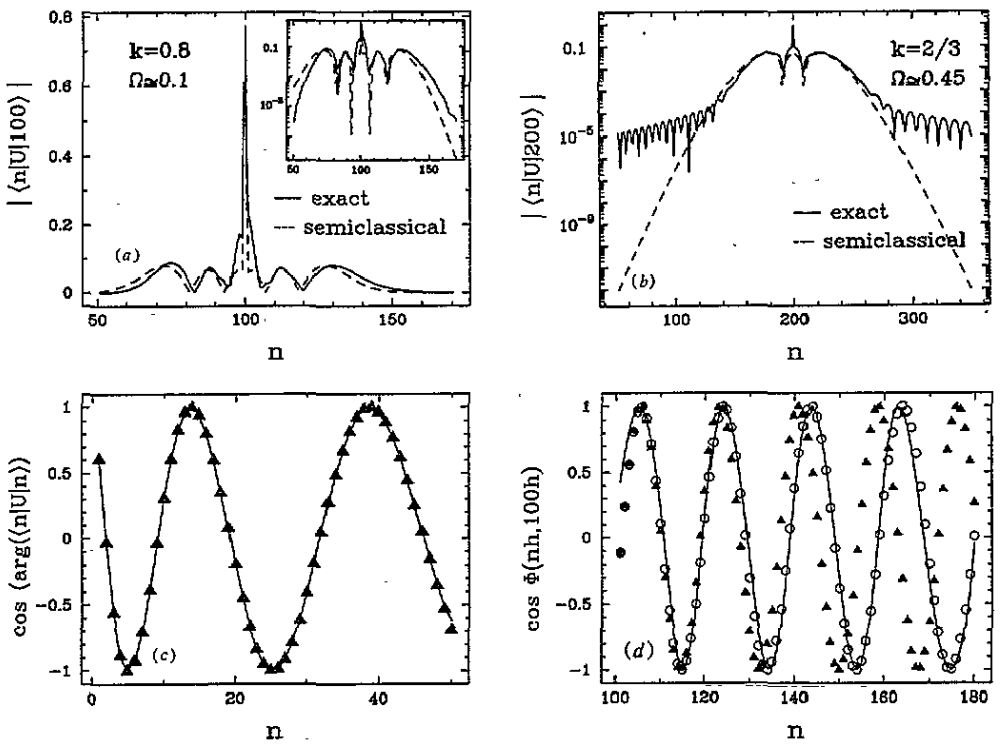

Figure 3. A comparison between the exact Floquet matrix and the semiclassical approximation. (*a*) The absolute value of the elements in a typical row (full curve, exact; broken curve, semiclassical), for $k = 0.8, \Omega \simeq 0.1$ and $\hbar = 3\pi$. (*b*) Same as (*a*) for $k = \frac{2}{3}, \Omega \simeq 0.45$ and $\hbar = 9\pi$, emphasizing the classically forbidden region outside the band. Note the small oscillations, not accounted for by the semiclassical approximation. (*c*) The phases of the diagonal elements (full curve, exact; triangles, semiclassical $\alpha n^{2/3}$, with $\alpha = \pi/\Omega\hbar^{1/3}$), for $k = 2.0, \Omega \approx 1.35$ and $\hbar = 3\pi$. (*d*) The phases of the off-diagonal matrix elements in line 100, for $k = 2.0, \Omega \approx 0.45$ and $\hbar = 3\pi$. Full curve, exact; triangles, semiclassical as given by (3.14); circles, semiclassical with $\epsilon(n)(n-m)$ replaced by $\mathcal{H}_0(n) - \mathcal{H}_0(m)$.

A comparison between the semiclassical result (3.28) and the exact Floquet matrix is presented in figure 3. The exact matrix was calculated using a numerical method suggested by Peskin and Moiseyev [49], based on the extended Hilbert space method [50]. The absolute values of the matrix elements in a typical row are plotted in figure 3(*a*). The band structure, beyond which a sharp exponential decrease of the elements occurs, agrees well with the semiclassical approximation. The oscillations of the Bessel function are seen to account nicely for the structure inside the band. The semi-logarithmic scale of the inset emphasizes these features. Figure 3(*b*) shows a similar comparison, for different parameters, emphasizing the classically forbidden region. It is seen that while the semiclassical matrix predicts a factorial decay as a function of n, the numerically calculated matrix, in fact,

decreases much more slowly, with characteristic oscillations. The magnitude of these oscillations is very small (they cannot be detected on a regular scale plot) and their period of oscillation slowly increases in the row. These structures are a result of higher order corrections to the semiclassical approximation, and are left for further investigation. Figure 3(*c*) shows the cosine of the phase of the diagonal matrix elements. The slowly varying nature of the phase is clearly seen. In figure 3(*d*) the cosine of the phase of the off-diagonal matrix elements is presented. The exact phase is compared with the semiclassical result (3.14), and with the value obtained when $\omega_0(n\bar{\hbar})(n\bar{\hbar} - m\bar{\hbar})$ in (3.14) is replaced by $E_n - E_m$. These two expressions are equivalent within the framework of the semiclassical approximation. It should be mentioned that the agreement between the exact calculation and the semiclassical approximation (3.28) improves as the size of the matrix is enlarged, and best agreement is found far from the edges of the matrix, in the vicinity of the centre of the band. The largest matrix size in the exact calculations is 400. The value of $\bar{\hbar}$ used here is $\bar{\hbar} = c_p c_x = 3\pi q\mathcal{E}_0/\sqrt{m}$, corresponding to $\tilde{\hbar} = 1$. For $q = 1$ and $m = 1$ it takes the value $\bar{\hbar} = 3\pi\mathcal{E}_0$.

The quasi-energies λ of the Floquet operator $\hat{U}$, and the corresponding eigenstates $|\psi_\lambda\rangle$, are defined by the equation

$$\hat{U}|\psi_\lambda\rangle = \mathrm{e}^{-\mathrm{i}2\pi\lambda}|\psi_\lambda\rangle\,. \tag{3.36}$$

In the unperturbed n-representation, we denote the quasi-energy states by $\psi(n)$ and suppress their λ-dependence. Typical states are shown in figure 4. The eigenstates of the exact matrix are compared to those of the approximation (3.28). A most striking feature of this function is the existence of a ladder of sharp peaks. A good agreement is found with the semiclassical eigenstates, concerning both the positions of these peaks, and the amplitude superimposed on the peak structure. Similar peaks were also seen in the steady state distribution obtained from evolving the system numerically [40]. The steps in the ladder are of an approximately $\bar{\hbar}$ energy interval which corresponds to a one-photon transition, and were therefore termed 'photonic states'. This ladder of peaks was also observed in numerical calculations for the driven hydrogen atom. For small external fields, such that classical perturbation theory is applicable with the field strength as the small parameter, this effect has a general theoretical explanation. It has been shown [33] that for a general bound system in a high-frequency field, the long-time transition amplitudes between unperturbed action variables obey an approximate selection rule (called a 'quasi-resonance'), corresponding to these one-photon transitions.

From the general structure of the semiclassical matrix (3.28), the following simple explanation for the quasi-resonance phenomenon emerges, without the need to rely on perturbation theory in the driving k. Consider first a matrix made up of the diagonal elements only. Each of the eigenstates of this matrix, corresponding to a given quasi-energy λ_n, is peaked on one site, n, which satisfies $\frac{1}{\bar{\hbar}}\mathcal{H}_0(n\bar{\hbar}) - \lambda_n = j$, where j is an integer. There are typically many values of n with λ_n nearly degenerate, so that there are many nearly degenerate states corresponding to a quasi-energy $\lambda \approx \lambda_n$, with peaks spaced at distances

$$\Delta n = \left(\frac{\partial\mathcal{H}_0}{\partial(n\bar{\hbar})}\right)^{-1} = 3\Omega(n\bar{\hbar})^{1/3} = [\epsilon(n\bar{\hbar})]^{-1}\,. \tag{3.37}$$

Now treating the off-diagonal terms in (3.28) as a perturbation (since they are small in the high-frequency limit), the degeneracy between the different values of n is lifted, and combinations of the peaked states are formed; this is the photonic ladder. It should be noted that this is an effect of the slow variation of $\mathcal{H}_0$ as a function of n. In other words, this

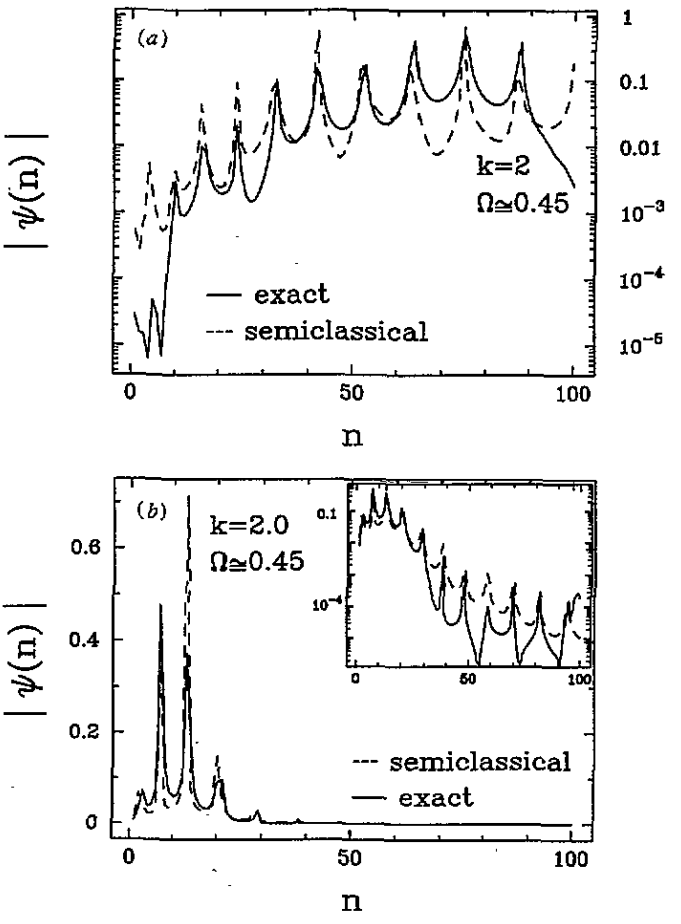

Figure 4. Typical eigenstates of the Floquet matrix (full curve) as compared to those of the semiclassical approximation (broken curve), for $k = 2.0$, $\Omega \approx 0.45$ and $\hbar = 3\pi$. The semi-logarithmic inset stresses the amplitude superimposed on the peak structure.

is because at high unperturbed energies the field becomes of high frequency, i.e. $\epsilon \to 0$. Consider, for example, a general model for $\mathcal{H}_0$,

$$\mathcal{H}_0(n) = \frac{C}{\Omega}(n\hbar)^\alpha \tag{3.38}$$

with α and C positive constants. Then according to the above reasoning, the positions of the quasi-resonances are spaced at

$$\Delta n = \frac{\Omega}{C\alpha}(n\hbar)^{1-\alpha}. \tag{3.39}$$

Therefore, the peaks are well defined asymptotically, namely they are separated by a distance larger than unity, only for $\alpha < 1$, where the phase of free propagation is a slowly varying function of n. Thus one obtains a simple explanation of the quasi-resonances only in terms of the unperturbed energy spectrum and the existence of a small perturbation by the off-diagonal terms of the Floquet operator. In our case the magnitude of these elements is proportional to ϵ. The detailed form of the off-diagonal terms, in particular, their phases, is not important for the existence of the photonic states. This picture is supported by

the fact that the position of the quasi-resonance ladder is continuous as a function of the quasi-energy λ; this fact is seen in the numerically calculated eigenstates of (3.28).

The condition for the existence of the photonic states can be formulated in terms of the characteristics of the binding potential. Consider a system described by the Hamiltonian

$$\mathcal{H}_0(x, p) = \frac{1}{2\Omega}p^2 + \frac{1}{\Omega}V(x) + kx\cos(t) \tag{3.40}$$

where $V(x)$ is a potential well in the form of a power law $V(x) \sim x^\sigma$, with $\sigma > 0$. Then in terms of the action variable n the energy levels are asymptotically $E_n \sim n^\alpha$, where $\alpha = 2\sigma/(\sigma + 2)$. The external field is therefore asymptotically of high frequency for wells with a power $\sigma < 2$, leading to $\alpha < 1$, and for these it is expected that the photonic states appear at high enough energy.

In the next section, an exact solution for the eigenstates will be found on a local scale, under certain conditions. This will provide a more quantitative description of the quasi-resonances beyond the heuristic explanation presented here, which includes their shape, average width and fluctuations in the width. In addition, it will enable the explanation of the larger scale structures observed in the numerical calculations, as well as the justification of some assumptions leading to previous results about the asymptotic decay of the eigenstates.

4. Investigation of the quasi-energy states

In this section the nature of the eigenstates of the matrix (3.28) will be studied. The properties of these functions will be considered on several scales, from the scale of the single quasi-resonance, to that of characteristic decay of the states. A connection between our picture and previous works will be made, and some assumptions leading to previous results concerning the asymptotic behaviour of the states will be justified. Many of the results of this section follow from the exact solution of a local linearized approximation of the semiclassical eigenvalue equation. The resulting model and its solution are presented in subsection 4.1. The structure of the single quasi-resonance predicted by the linearized solution is studied in subsection 4.2. In particular, it is argued that in the semiclassical limit the eigenstates of the full (nonlinear) system are combinations of such quasi-resonances. The resulting asymptotic behaviour of the eigenstates is explored in subsection 4.3, while the intermediate structure, covering many quasi-resonances but not asymptotic, is studied in subsection 4.4.

4.1. The linearized model and its exact solution

The eigenvalue equation for the Floquet operator in the n representation is

$$\sum_{n'} U_{n,n'}\psi_{n'} = \mathrm{e}^{-\mathrm{i}2\pi\lambda}\psi_n \,. \tag{4.1}$$

(Recall that in our units, the field period is 2π.) In the semiclassical initial-value representation used here, the matrix elements can be written as (see equations (3.8), (3.9) and (3.28))

$$U_{n,n'} = \frac{1}{2\pi}\int_0^{2\pi} \mathrm{e}^{\frac{\mathrm{i}}{\hbar}F(\theta)}\,\mathrm{d}\theta \tag{4.2}$$

where

$$\frac{1}{\hbar}F(\theta) = -\frac{2\pi}{\hbar}\mathcal{H}_0(n\hbar) + 2\pi\epsilon(n - n') + \theta(n - n') + \frac{R}{\hbar}(\cos\tau^*(\theta) - 1)\,. \tag{4.3}$$

Here ϵ and R are implicitly n-dependent quantities, and τ^* was extended to include the whole θ region, as in the previous section. Denoting $r=n'-n$, one can write the eigenvalue equation in the following form:

$$\sum_{r=-\infty}^{\infty} U_{n,n+r}\psi_{n+r} = \sum_{r=-\infty}^{\infty} U_{n,n+r}\,\mathrm{e}^{\mathrm{i}\hat{\theta}r}\psi_n = \mathrm{e}^{-\mathrm{i}2\pi\lambda}\psi_n \tag{4.4}$$

where the sum over r has been extended to $-\infty$. This is justified for large n, since in this case the tail of the sum includes exponentially small contributions. Also the translation operator on the lattice $\mathrm{e}^{\mathrm{i}\hat{\theta}}$, defined by $\mathrm{e}^{\mathrm{i}\hat{\theta}}\psi_n = \psi_{n+1}$, was introduced. Now using the expression for the matrix elements, the sum over r in (4.4) can be performed:

$$\sum_{r=-\infty}^{\infty} U_{n,n+r}\,\mathrm{e}^{\mathrm{i}\hat{\theta}r} = \mathrm{e}^{-\mathrm{i}\frac{2\pi}{\hbar}\mathcal{H}_0(n\hbar)}\frac{1}{2\pi}\int_0^{2\pi}\sum_{r=-\infty}^{\infty}\mathrm{e}^{-\mathrm{i}(2\pi\epsilon+\theta)r+\frac{\mathrm{i}}{\hbar}R(\cos\tau^*(\theta)-1)}\mathrm{e}^{\mathrm{i}\hat{\theta}r}\,\mathrm{d}\theta\,. \tag{4.5}$$

Since R is a slowly varying function of n ($R\sim n^{1/3}$), it will be assumed that acting on it with the translation operator does not change it much, and therefore the function and the operator commute. Since the values of r effectively participating in the sum are within a bandwidth of the matrix, this approximation means that the function $R(\cos\tau^*-1)/\hbar$ does not change much within one bandwidth. Explicitly, this condition is

$$\eta_1 \equiv \frac{8k^2}{9\pi^2\Omega^3\hbar} \ll 1\,. \tag{4.6}$$

Then, the summation of (4.5) yields the following eigenvalue equation:

$$\mathrm{e}^{-\mathrm{i}\frac{2\pi}{\hbar}\mathcal{H}_0(n\hbar)}\,\mathrm{e}^{\frac{\mathrm{i}}{\hbar}R[\cos\bar{\tau}(\hat{\theta})-1]}\psi_n = \mathrm{e}^{-\mathrm{i}2\pi\lambda}\psi_n \tag{4.7}$$

where $\bar{\tau}=\tau^*(\theta-2\pi\epsilon)$, or in explicit form

$$\bar{\tau}(\theta) = \begin{cases} \dfrac{2\pi\epsilon-\theta}{\epsilon} & \theta<2\pi\epsilon \\ 0 & \theta>2\pi\epsilon\,. \end{cases} \tag{4.8}$$

Equation (4.7) is the eigenvalue equation for a kicked system, with a 'kinetic energy' term which is proportional to $n^{2/3}$, and a kick that depends adiabatically on n.

Equation (4.7) can be solved locally, if one exploits the slowly varying nature of the 'kinetic' energy and approximates it by a linear function

$$\mathcal{H}_0(n\hbar) = \frac{1}{2\Omega}(n\hbar)^{2/3} \approx \mathcal{H}_0(n_0\hbar) + \left(\frac{\partial\mathcal{H}_0}{\partial n}\right)(n-n_0) = \mathcal{H}_0(n_0\hbar)+\epsilon l\hbar \tag{4.9}$$

where $l=(n-n_0)$. This is a good approximation as long as the correction is much smaller than π, namely in a region around n_0 of size δn satisfying

$$\delta n \ll 3\sqrt{\Omega\hbar^{1/3}}n_0^{2/3}\,. \tag{4.10}$$

This region increases as $n_0\to\infty$. In a region of this size in the vicinity of n_0, the function $\zeta[\cos\bar{\tau}(\hat{\theta})-1]$ can be considered to be independent of l, as long as (4.6) holds. Therefore, in this approximation we have the eigenvalue equation of the linear rotor,

$$\mathrm{e}^{-\mathrm{i}2\pi\epsilon\hat{l}}\,\mathrm{e}^{-\frac{\mathrm{i}}{\hbar}V(\hat{\theta})}\psi_\lambda = \mathrm{e}^{-\mathrm{i}2\pi(\lambda-\lambda_0)}\psi_\lambda \tag{4.11}$$

with a 'kicking potential'

$$V(\theta) = \begin{cases} -R[\cos(\theta/\epsilon)-1] & \theta<2\pi\epsilon \\ 0 & \theta>2\pi\epsilon \end{cases} \tag{4.12}$$

and a constant term which shifts the quasi-energies: $\lambda_0 = \mathcal{H}_0(n_0\hbar)/\hbar$. The operator $\hat{l}$ is the momentum conjugate to $\hat{\theta}$. This problem has an exact closed solution in the form of a series in the θ representation [34]

$$\langle\theta|\psi_\lambda\rangle = \exp \mathrm{i}\left\{\theta\mu + \frac{1}{\hbar}\sum_{m\neq 0} V_m \frac{\mathrm{e}^{\mathrm{i}m\theta}}{\mathrm{e}^{-\mathrm{i}m2\pi\epsilon} - 1}\right\} \tag{4.13}$$

where $V(\theta) = \sum V_m \mathrm{e}^{\mathrm{i}m\theta}$, and μ is an integer defined by the equation

$$2\pi(\lambda - \lambda_0) \equiv \frac{1}{\hbar}V_0 + \mu 2\pi\epsilon \,[\mathrm{mod}\, 2\pi]\,. \tag{4.14}$$

In our case, we have for the Fourier components

$$V_m = \frac{-R}{2\pi}\mathrm{e}^{-\mathrm{i}\pi m\epsilon}\sin(\pi m\epsilon)\frac{2/\epsilon^2}{m(m^2 - 1/\epsilon^2)} \qquad V_0 = R\epsilon \tag{4.15}$$

and thus the function of (4.13) is found to be

$$\langle\theta|\psi_\lambda\rangle = \exp \mathrm{i}\left\{\theta\mu + \sum_{m=1}^{\infty}\frac{\zeta}{2\pi}\frac{2/\epsilon^2}{m^3 - m/\epsilon^2}\sin(m\theta)\right\} \tag{4.16}$$

where $\zeta = R/\hbar$. Note that the Fourier series decays asymptotically as $1/m^3$. This is related to the fact that the potential $V(\theta)$ has a discontinuous second derivative. The sum in the exponent can be summed exactly, and the function can be written explicitly in the $|l\rangle$ representation,

$$\langle l|\psi_\lambda\rangle = \mathrm{e}^{\mathrm{i}(\mu-l)\pi}\sum_{-\infty}^{\infty} J_m(B)\frac{\sin[(\mu-l)\pi + \zeta/2 - m\pi/\epsilon]}{[(\mu-l)\pi + \zeta/2 - m\pi/\epsilon]} \tag{4.17}$$

where $B = \zeta/2\sin(\pi/\epsilon)$. Some details of the derivation are presented in appendix C.

The function in (4.17) is composed of a chain of narrow peaks, which is just the ladder of quasi-resonances, or photonic states. In addition, it has a characteristic width, determined by the width of the Bessel function. Since our solution is only local, its typical width should be compared to the size of the region over which the linearization holds (condition (4.10)). The local approximation is consistent if the function decays within the regime of linearization, since otherwise a strong sensitivity to the boundaries of the region is expected. The condition for consistency of the linearized solution is

$$\eta_2 \equiv \frac{k^2}{9\pi^2\hbar\Omega^3} \ll 1\,. \tag{4.18}$$

Note that this condition is compatible with (4.6), namely with the approximation that led to the effective kicking propagator.

In the rest of this section the properties of the function (4.17) will be studied, and will be tested numerically against the eigenstates of the semiclassical matrix (3.28). The full wavefunctions will be constructed by matching various regions where (4.10) holds. The main consequence of this procedure is that the eigenstates are combinations of sharply localized quasi-resonances. This result will be used to justify and extend a previously used method, in order to draw conclusions about the asymptotic nature of the states.

4.2. Structure of single quasi-resonances

According to the local solution (4.17), the quasi-resonances have the shape of the function $\mathrm{sinc}(x) \equiv \sin(x)/x$ on a lattice, separated by a distance of approximately $1/\epsilon$.

Figure 5 shows a single quasi-resonance in an eigenstate of the semiclassical matrix (3.28), compared to the same quasi-resonance in the linear approximation to this function, equation (4.17). The value of μ was found numerically from (4.14). The position of the peak, as well as its shape, fits well to the theory. For the parameters of figure 5, the condition under which the theory was developed are fulfilled; $\eta_1 \approx 0.19$. The condition for the consistency of the linear solution $\eta_2 \ll 1$ is similarly satisfied. It should be noted, however, that good agreement on the scale of the single quasi-resonance is found by the same calculations also for parameters where these inequalities are violated.

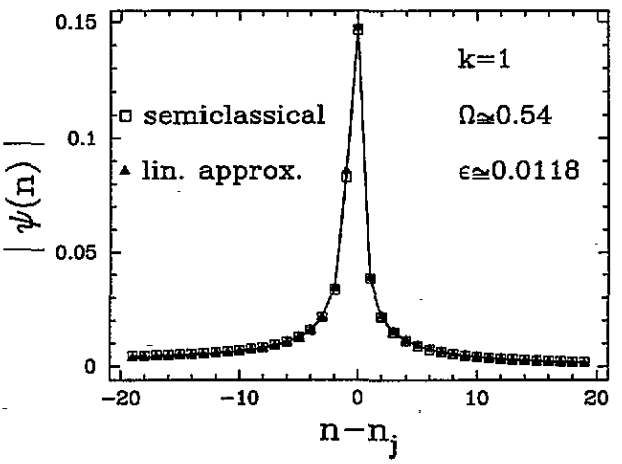

Figure 5. A comparison between a quasi-resonance in an eigenstate of the semiclassical matrix (squares), and that of the corresponding eigenstate of the local equation, equation (4.17) (triangles), for $k = 1$, $\Omega \approx 0.54$, $\hbar = 3\pi$ and $n_j = 14\,970$.

In principle, one would expect that under the conditions of validity (4.18), the linearized solution will fit the semiclassical eigenstate over a range of many quasi-resonances in the asymptotic limit. In practice, however, the increasing bandwidth limits the size of n_0 around which the semiclassical matrix can be constructed and diagonalized numerically. Therefore, numerical calculations can be performed only in a region of parameters where the linearized solution is valid on relatively short scales. Note, that the local solution (location of resonance, its shape and height) depends sensitively on the changes of the local parameters $1/\epsilon$ and ζ, since they appear in the argument of a trigonometric function (see equation (4.17)). For example, in figure 5, the change in these parameters between neighbouring quasi-resonances is of order 0.1π. The peaks next to the one shown in the figure, do not fit the local solution so well in their shape and height.

In order to go beyond the region of validity of the linear approximation, i.e. to 'sew together' the different regions of linearization, we now construct a local approximation for the wavefunction corresponding to a quasi-energy λ near the jth quasi-resonance. Starting from the solution to the local linearized problem (equation (4.17)), with a quasi-energy λ, we consider the argument of the sinc at a quasi-resonance peak. This peak, denoted by l_j, is determined by the condition that the argument is closest to zero. We define the deviation

from zero, $\delta_j\pi$, by the following equation:

$$(\mu - l_j)\pi + \zeta/2 - m\pi/\epsilon = \delta_j\pi\,. \tag{4.19}$$

By definition, $|\delta_j| < \frac{1}{2}$. Substituting the expression (4.14) for μ,

$$2\pi\epsilon\mu = 2\pi(\lambda - \lambda_0) - \frac{V_0}{\hbar} + 2\pi r \qquad r \in \mathcal{Z} \tag{4.20}$$

and using the explicit value (4.15) for V_0, we find that δ_j satisfies the following equation:

$$\epsilon l_j\hbar = \hbar(\lambda - \lambda_0) + j\hbar - \epsilon\hbar\delta_j \tag{4.21}$$

where $j = r - m$. Recalling that $\epsilon l_j\hbar$ is the unperturbed energy of the linearized model at the peak l_j, one sees that in the framework of this model δ_j is just the detuning of this energy from exact resonance with the electric field, normalized by the level spacing $\epsilon\hbar$. The quasi-energy sets the origin of the quasi-resonance ladder, and the peaks are located at equal distances $j\hbar$ in energy, with a mismatch $\epsilon\hbar\delta_j$. The quasi-resonances are labelled by j which is their position on this ladder.

Now consider an eigenstate corresponding to a quasi-energy λ, of the original (not linearized) problem, with the slowly varying energy $\sim n^{2/3}$. In the close vicinity of a given quasi-resonance, it can be approximated locally by an eigenstate of the linear kicked rotor (4.11), with the local values of ϵ, ζ and λ_0, and with the given value of λ. The quasi-resonance at n_j will then be described by a sinc function with δ_j satisfying the following equation:

$$E_{n_0} + \epsilon(n_j - n_0)\hbar = \hbar\lambda + j\hbar - \epsilon\hbar\delta_j\,. \tag{4.22}$$

This equation follows from (4.21), since $l_j = (n_j - n_0)$ and $E_{n_0} = \lambda_0\hbar$. If the linearization centre n_0 is close enough to the quasi-resonance, and for large enough n_0, one may approximate $\hbar\epsilon \approx (\partial E_n/\partial n)_{n_j}$ and $E_{n_0} + \epsilon(n_j - n_0)\hbar \approx E_{n_j}$, with a correction term that is of higher order in ϵ, so that the parameter characterizing the quasi-resonance centred at action n_j is just δ_j satisfying

$$E_{n_j} = \hbar\lambda + j\hbar - \delta_j\left(\frac{\partial E_n}{\partial n}\right)_{n=n_j}\,. \tag{4.23}$$

Thus, the eigenvalue λ sets the origin of the quasi-resonance ladder corresponding to the state, and the quasi-resonances are numbered by their position j on this ladder. Each is described approximately by a sinc function,

$$Q_j^{\lambda}(n) = \frac{\sin[\pi(n - n_j + \delta_j)]}{\pi(n - n_j + \delta_j)} \tag{4.24}$$

characterized by the peak position n_j and the normalized detuning δ_j of (4.23). This equation was obtained in a region where linearization holds around E_{n_0}. Now the centre of linearization can be varied, resulting in a local relation between E_{n_j}, j and δ_j.

The sequence of peak positions n_j and normalized detunings δ_j for a sequence of neighbouring quasi-resonances is estimated by writing, near the jth quasi-resonance, the energy as a function of a continuous action:

$$j\hbar + \lambda\hbar \;=\; E_{n_j} + \left(\frac{\partial E_n}{\partial n}\right)_{n_j}\delta_j \;\cong\; E(n_j + \delta_j) \;=\; \frac{1}{2\Omega}(\hbar(n_j + \delta_j))^{2/3}\,. \tag{4.25}$$

Inverting this relation, one finds that

$$n_j = \mathrm{int}\left\{\frac{[2\Omega\hbar(\lambda + j)]^{3/2}}{\hbar}\right\} \tag{4.26}$$

and

$$\delta_j = \mathrm{frac}\left\{\frac{[2\Omega\hbar(\lambda + j)]^{3/2}}{\hbar}\right\} \tag{4.27}$$

where $\mathrm{int}\{x\}$ is the integer part of x and $\mathrm{frac}\{x\}$ its fractional part. Therefore, the δ_j form a pseudorandom sequence as a function of the quasi-resonance number j [28, 29], with a uniform distribution in $[-\frac{1}{2}, \frac{1}{2}]$.

In figure 6, sections of typical quasi-energy states are compared to sequences of the single-resonance approximations (4.24), with parameters n_j and δ_j as predicted by (4.26) and (4.27). In figure 6(a) the state was obtained by diagonalization of the numerically calculated exact Floquet matrix, whereas in figures 6(b) and (c) the states are those of the semiclassical matrix (3.28). The value of λ used in (4.26) and (4.27) was obtained by a fitting which minimizes the mean-square deviation from the numerical state. It was found in the close vicinity of the numerical eigenvalue corresponding to this state. The difference was of the order of 10^{-3} for figure 6(a), and 10^{-2} for figures 6(b) and (c). The reason for this difference is probably the non-semiclassical behaviour in the small-n region for the exact matrix, and the deviation from unitarity of the semiclassical matrix. The maximum of each sinc was normalized to the amplitude of the wavefunction at the quasi-resonance peak. Thus the calculation only tests the assumption that the eigenstates are formed by the sequence of sinc functions (4.24) with the values of n_j and δ_j predicted by (4.26) and (4.27). It does not address the question of their amplitudes. For clarity, only a small part of the n-values are shown, but a similar agreement holds throughout the whole basis used. In the case of the exact matrix, the agreement improves for higher values of n, as expected. The integrated square difference between the state obtained by diagonalization and the chain of local approximants (4.24) is of the order 10^{-4} for figure 6(a), and 10^{-2} for (b) and (c). The quasi-resonance structure of the shape (4.24) with the values of n_j and δ_j as predicted by (4.26) and (4.27), is found also for eigenstates of blocks of the semiclassical matrix which are smaller than the bandwidth $b(n)$, in a region of parameters where the condition (4.6) is strongly violated. This is the case for the parameters of figure 6(c), where $\eta_1 \approx 19$. We conclude that this structure is not sensitive to boundary conditions, giving an additional support to the 'sewing' procedure for the wavefunctions.

On the basis of the local linearization, and with the support of numerical tests, we thus conclude that the quasi-energy state in the n representation can be constructed as a linear combination of the functions $Q_j^\lambda(n)$, with a sequence of n_j and δ_s satisfying (4.26) and (4.27). Their relative weights cannot be determined from the linearized approximation, since these represent the structure of the function over a wide range, where the linearization does not hold. Note that the functions $Q_j(n)$ are not orthogonal, and their overlap sum is

$$\sum_n Q_j^\lambda(n) Q_{j'}^\lambda(n) = \frac{\sin[(n_{j'} - n_j + \delta_j - \delta_{j'})\pi]}{(n_{j'} - n_j + \delta_j - \delta_{j'})\pi}. \tag{4.28}$$

From equation (4.27) it is clear that the difference between various values of δ_j is, in general, of order unity. Equation (3.37) implies that

$$\epsilon|n_j - n_{j'}| > 1 \qquad \text{for} \quad j \neq j' \tag{4.29}$$

consequently the magnitude of the overlap sum is bounded by $\epsilon(I = n_m\hbar)$, where $m = \min(j, j')$. It decreases as a function of $|j - j'|$. Orthogonality is approached in the limit $\epsilon \to 0$. The eigenstates will thus be assumed to take the approximate form

$$\psi_n^\lambda = \sum_j A_j^\lambda Q_j^\lambda(n) \tag{4.30}$$

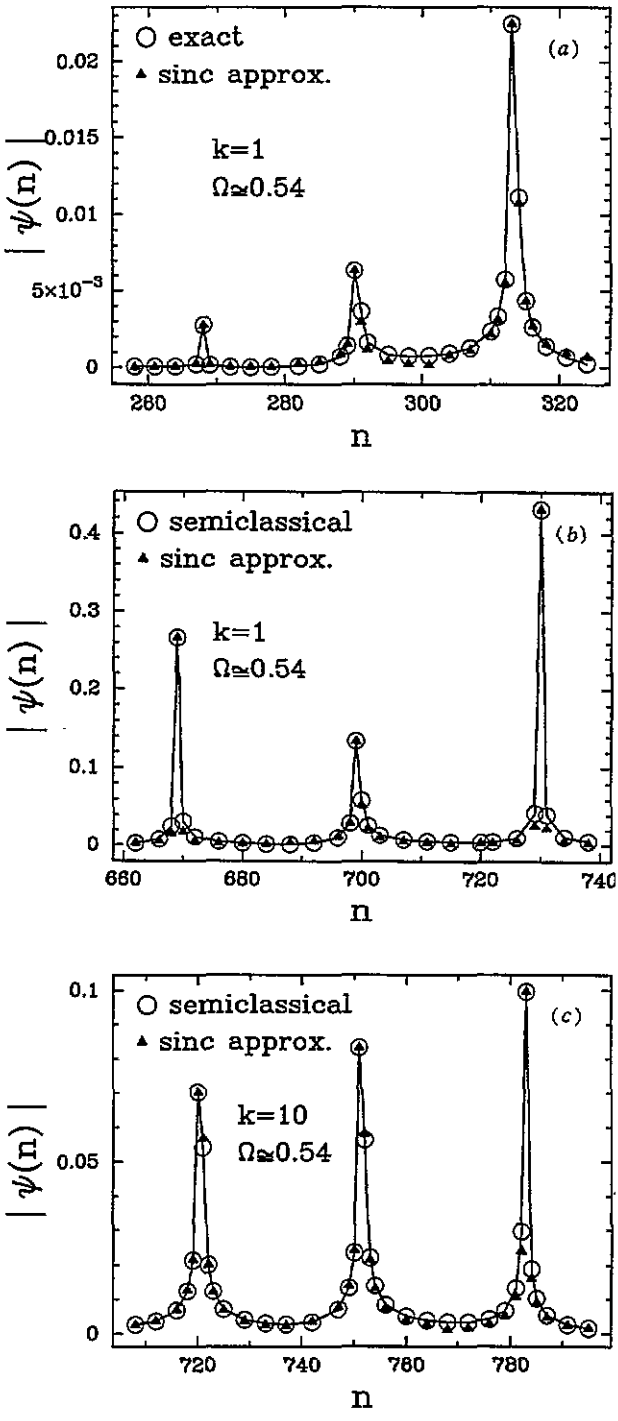

Figure 6. Test of the general form (4.30), with the parameters δ_j satisfying (4.27) and with arbitrary amplitudes A_j^{λ}, for the eigenstates of (*a*) the exact matrix, and (*b*) and (*c*) the semiclassical matrix, for $\Omega \sim 0.54$ and $\hbar = 3\pi$. A small portion of the state is shown in the figure, but a similar agreement holds for the whole n-basis used. For the parameters of (*c*), the conditions of the theory are strongly violated, $\eta_1 \approx 19$ (see equation (4.6)).

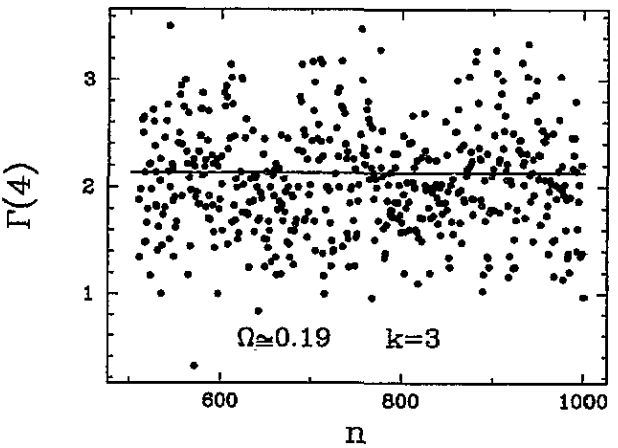

Figure 7. The width $\Gamma(4)$ of quasi-resonances as a function of their position n. The data are collected from many eigenstates of the semiclassical matrix with $k = 3$, $\Omega \approx 0.19$ and $\hbar = 6\pi$. The full curve shows the average as predicted by (4.31) with δ uniformly distributed.

where $Q_j(n)$ is defined by (4.24), with parameters n_j and δ_j satisfying (4.26) and (4.27). The expansion coefficients A_j^λ form the slowly varying envelope superimposed on these quasi-resonances. Because of the pseudorandom phases of the sinc functions $Q_j^\lambda(n)$, at any given point only one or two functions contribute considerably to ψ_n^λ. Therefore the amplitudes A_j^λ determine the long-range behaviour of the state ψ_n^λ. In the next subsection, an approximate eigenvalue equation for the amplitudes A_j^λ will be constructed.

The description of the eigenstates by a combination of sinc functions was verified numerically for several states. In order to test it for a large number of states, the width of single quasi-resonances will be studied statistically. Since the sinc function decays slowly away from its peak, it is convenient to define its width $\Gamma(D)$ as the number of unperturbed states included in $1/D$ of its peak value, where D is some positive constant. It is seen from (4.24) that this width is predicted to be independent of parameters, and is only a result of the deviation of the argument of the sinc from an integer multiple of π. This can be related intuitively to the fact that the typical time scale for transitions in this problem is the unperturbed classical period $2\pi/\epsilon$, since transitions occur only near the wall (see also (3.30)). By uncertainty, this defines a linewidth in energy of $\Delta E \sim \hbar\epsilon$, and taking into account the density of states, $(\partial E_n/\partial n) = \hbar\epsilon$, the corresponding width in n space is found to be of order one. Note that the use of Rabi's formula [32] is not justified here since many levels are involved in the transitions. Indeed, Rabi's formula gives a typical width of the quasi-resonances which depends on parameters, and, in particular, grows as $n^{1/3}$. Figure 7 presents the widths $\Gamma(4)$ of quasi-resonances as a function of their peak position in n. The data are accumulated from many different eigenstates of the semiclassical matrix (3.28). It is seen that the widths fluctuate around a mean value, with no systematic dependence on n. The full curve is the average as predicted by the calculation presented in what follows.

Using equation (4.24) and the definition $\Gamma(D)$ for the width, one finds that

$$\Gamma(D) = 1 + \lfloor |\delta|(D-1) \rfloor + \lfloor |\delta|(D+1) \rfloor \tag{4.31}$$

where $\lfloor x \rfloor$ is the integer part of x, while δ is the value of the detuning δ_j for the quasi-resonance in question. The derivation of this function is described in appendix D. Now the statistical distribution of widths is obtained from this function for δ uniformly distributed in the interval $\left[-\frac{1}{2}, \frac{1}{2}\right]$. The mean value of this distribution is the full curve depicted

in figure 7. The predicted distribution was tested numerically for the quasi-resonances in the eigenstates of the semiclassical matrix. The results are shown for $D = 8$ in figure 8. Note that the distribution is non-monotonic, and exhibits a non-trivial behaviour which the semiclassical data closely follow. It is, however, a single-resonance approximation; effects of neighbouring resonances on each other are ignored, and therefore larger deviations are expected for high values of $\Gamma(8)$. For the same reason, the whole description is valid only for values of D much smaller than the separation between resonances.

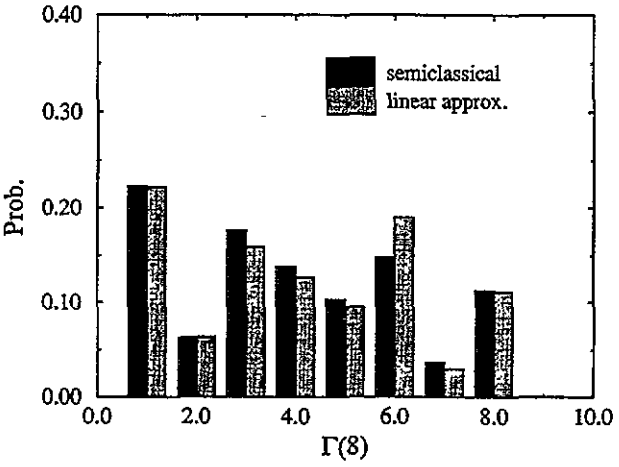

Figure 8. Data collected from many eigenstates of the semiclassical matrix (dark bars) with $k = 1$, $\Omega \approx 0.54$ and $\hbar = 3\pi$, are compared to the analytical prediction, equation (4.31) with δ uniformly distributed (light bars).

4.3. The asymptotic behaviour of the eigenstates

The results of the previous subsections can be used to justify and extend the procedure presented by de Oliveira *et al* [32], where the eigenvalue equation for the Floquet Hamiltonian was projected onto the photonic states. We first introduce the Floquet Hamiltonian corresponding to the unperturbed system $\mathcal{H}_0$:

$$\hat{\mathcal{K}}_0 = \mathcal{H}_0 - i\hbar\frac{\partial}{\partial\tau}. \tag{4.32}$$

It has a basis of eigenstates

$$|n, j) = |n\rangle e^{-ij\tau} \tag{4.33}$$

where $|n\rangle$ are the eigenstates of $\mathcal{H}_0$, with corresponding eigenvalues $(E_n - \hbar j)$. Now the full Floquet Hamiltonian is $\hat{\mathcal{K}} = \mathcal{H} - i\hbar\partial/\partial\tau$, with $\mathcal{H}$ the full time-dependent Hamiltonian. We write the eigenvalue equation for the operator $\hat{\mathcal{K}}$ in the $|n, j)$ representation,

$$(E_n - \hbar j)\phi^{\lambda}_{n,j} + \frac{k}{2\Omega}\sum_{n'}\langle n|\hat{x}|n'\rangle\left[\phi^{\lambda}_{n',j+1} + \phi^{\lambda}_{n',j-1}\right] = \hbar\lambda\phi^{\lambda}_{n,j}. \tag{4.34}$$

where $\phi^{\lambda}_{n,j} = (n, j|\phi_\lambda)$. Note that to an eigenstate of $\hat{U}$ with eigenphase λ corresponds an eigenstate of $\hat{\mathcal{K}}$ with eigenvalue $\hbar\lambda$. In the unperturbed case, $k = 0$, the eigenstates are just δ-functions at sites n_j satisfying $\lambda = (E_{n_j}/\hbar - j)$. This sets the relation between the states $|n, j)$ and the states $|n\rangle$ for a given λ. The perturbation mixes different values of j corresponding

to approximately the same λ, to form the ladder of quasi-resonances; therefore the index j is identified as the quasi-resonance number. From the previous subsections, we know that for $k > 0$ the states are combinations of sinc-functions $Q_j(n)$ with amplitudes to be determined. We now use this knowledge to modify the method of [32], and construct an equation for these amplitudes. We introduce the following approximation for the wavefunction:

$$\phi^{\lambda}_{n,j} = A^{\lambda}_j Q^{\lambda}_j(n) = A^{\lambda}_j \frac{\sin[\pi(n - n_j + \delta_j)]}{\pi(n - n_j + \delta_j)} . \tag{4.35}$$

Using equation (4.23) for the relation between n_j and λ, equation (4.34) reduces to an approximate equation for the A^{λ}_j:

$$-A^{\lambda}_j \hbar \delta_j \epsilon_j \frac{\sin(\pi\delta_j)}{\pi\delta_j} + \frac{k}{2\Omega} \sum_{n'} \langle n_j|\hat{x}|n'\rangle \left[A^{\lambda}_{j+1} Q^{\lambda}_{j+1}(n') + A^{\lambda}_{j-1} Q^{\lambda}_{j-1}(n')\right] \approx 0 \tag{4.36}$$

where ϵ_j is the value of ϵ near the jth quasi-resonance. This is an approximate eigenvalue equation with a nearly vanishing eigenvalue. The matrix elements are known to be

$$\langle n|\hat{x}|n'\rangle = -\frac{\hbar^2}{(3\pi\Omega)^2} \frac{1}{(E_n - E_{n'})^2} . \tag{4.37}$$

We approximate $E_{n_j} - E_{n'} \approx \hbar - (n' - n_{j+1})\epsilon\hbar$, since the main contributions are from the states around the neighbouring quasi-resonances, whose peak-to-peak distance in energy is $\hbar$. The sums over n' in (4.36) can now be performed with the help of the relation

$$\sum_{M=-\infty}^{\infty} \frac{\sin[\pi(M+\delta)]}{\pi(M+\delta)} \frac{1}{(\hbar - M\epsilon\hbar)^2} = \frac{1}{\hbar^2(1+\delta\epsilon)^2} . \tag{4.38}$$

Near the jth quasi-resonance one finds, using the approximation $E_{n_j} \approx j\hbar$ (see equation (4.23)),

$$\hbar\epsilon_j = \left(\frac{\partial E_n}{\partial n}\right) \approx \frac{\sqrt{\hbar}}{3\Omega^{3/2}\sqrt{2j}} \tag{4.39}$$

consequently (4.36) takes the form

$$3\pi\sqrt{2} \left(\frac{\sin(\pi\delta_j)}{\sqrt{j}}\right) \left(\frac{\sqrt{\hbar}\Omega^{3/2}}{k}\right) A^{\lambda}_j + \left[\frac{A^{\lambda}_{j+1}}{(1+\delta_{j+1}\epsilon_{j+1})^2} + \frac{A^{\lambda}_{j-1}}{(1+\delta_{j-1}\epsilon_{j-1})^2}\right] \approx 0 . \tag{4.40}$$

This equation is very similar to (6) in [32], where a projection onto single n-states was used. The correction due to the finite width of the resonances results in the replacement of the diagonal part by a sine function (instead of a modulo function), and a correction to the off-diagonal hopping which vanishes in the asymptotic limit $\epsilon \to 0$. In deriving it, we have used the specific form of the eigenstates on a local scale, namely the locations and shapes of the quasi-resonances.

If $\sin(\pi\delta_j)$ were a random sequence, the exact results of [41] would ensure the existence of power-localized eigenstates for (4.40). The power would then be proportional to the square of the diagonal potential, implying in our case a power proportional to $(\hbar\Omega^3/k^2)$. Figure 9 shows the same calculation as presented in [32], but for the model of (4.40). Starting with an arbitrary initial vector $(A^{\lambda}_0, A^{\lambda}_1)$ and using the transfer matrix technique, one finds that the norm of the vector iterated a large number m of times, increases as m^{β}. The power β is expected to be related to the power of decay of the eigenstates of (4.40). It can be extracted from the following relation [32]:

$$\frac{1}{N} \sum_{m=1}^{N} \log\sqrt{(A^{\lambda}_m)^2 + (A^{\lambda}_{m+1})^2} = \text{constant} + \frac{\beta}{N} \sum_{m=1}^{N} \log m . \tag{4.41}$$

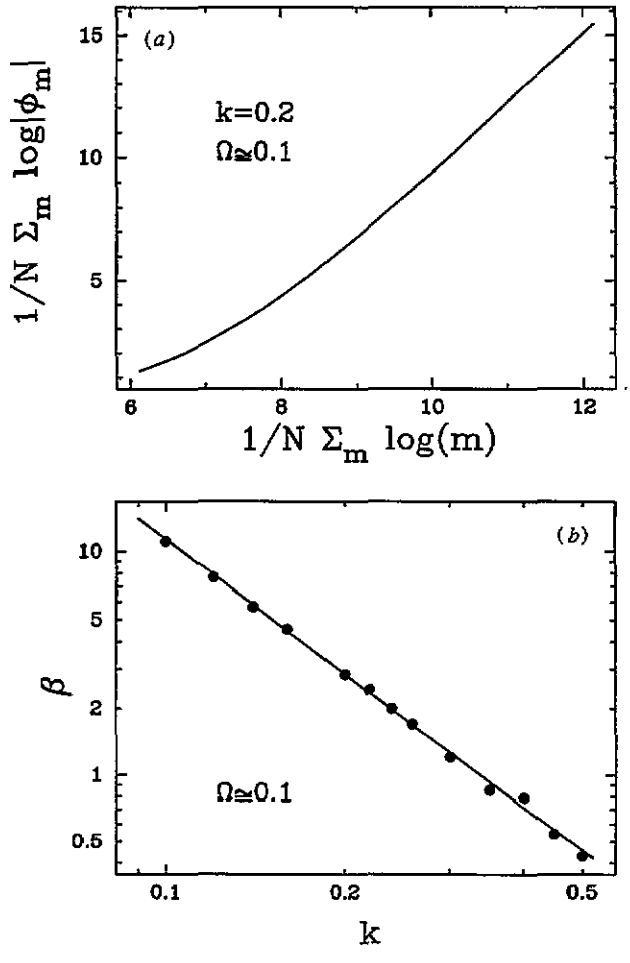

Figure 9. Results of the same calculations as in [32], but for the refined model (4.40). (*a*) The large-m behaviour of the norm of a vector under the action of transfer matrices corresponding to the model, for $k = 0.07, \hbar = 3\pi$ and $\Omega = 0.106$. The starting point for iterations was $n_0 = 800$ and the resulting power is $\beta \approx 6.2$. The graph is an average over 51 values of λ around $\lambda = 0$. (*b*) The dependence of the power of growth β on k. The best fit is $\ln \beta = (-2.02 \pm 0.02) \ln k - 3.5$.

An example of such a calculation is presented in figure 9(*a*). The dependence of β on k with $\Omega \approx 0.106$ held fixed, is plotted in figure 9(*b*). The best-fit power to the graph is -2.00 ± 0.03. This value is consistent with the results of [32, 41]. Thus, this calculation supports the assumption that the minor differences between our model (4.40) and the one of [41] do not alter the conclusions concerning the power-law decay of the eigenstates. These differences include the fact that the diagonal potential is pseudorandom instead of random, and that the hopping term is not constant but weakly dependent on position. Notice that this dependence decreases in the asymptotic limit $\epsilon \to 0$.

The conclusion of this analysis is thus identical to that of [32]: the eigenstates are predicted to be asymptotically power-law decaying, with a power

$$\beta = C_\beta \left(\frac{\hbar \Omega^3}{k^2} \right) \tag{4.42}$$

as a function of the quasi-resonance number j. As a function of n, the asymptotic decay is with a power of $(2\beta/3)$. The constant of proportionality C_β is found from numerical calculations to be approximately 10 (compared to 12.2 of [32]). Thus the critical field k_c for which the power of decay as a function of j is less than $\frac{1}{2}$ is $k_c \approx 4.47\sqrt{\hbar\Omega^3}$ (compared to $4.9\sqrt{\hbar\Omega^3}$ of [32]). Our analysis was based on detailed information concerning the local structure of the quasi-resonances in the state, and justifies most of the assumptions of [32].

4.4. A local-scale crossover

From the structure of the quasi-resonances and the shape of the semiclassical matrix, a crossover in the behaviour of the function on a local scale can be predicted. There are two basic length scales in action space: the bandwidth $b(n)$ of the Floquet matrix and the distance Δn between neighbouring quasi-resonances. Considering that transitions are most effective between quasi-resonant states, one can argue heuristically that in the region where the $b(n) < \Delta n$ transitions are less likely to occur [33]. In this regime, absorption of even one photon involves transition through a classically forbidden region. The phases at the quasi-resonances are pseudorandom and therefore exponential localization is expected in this region. The condition for this is

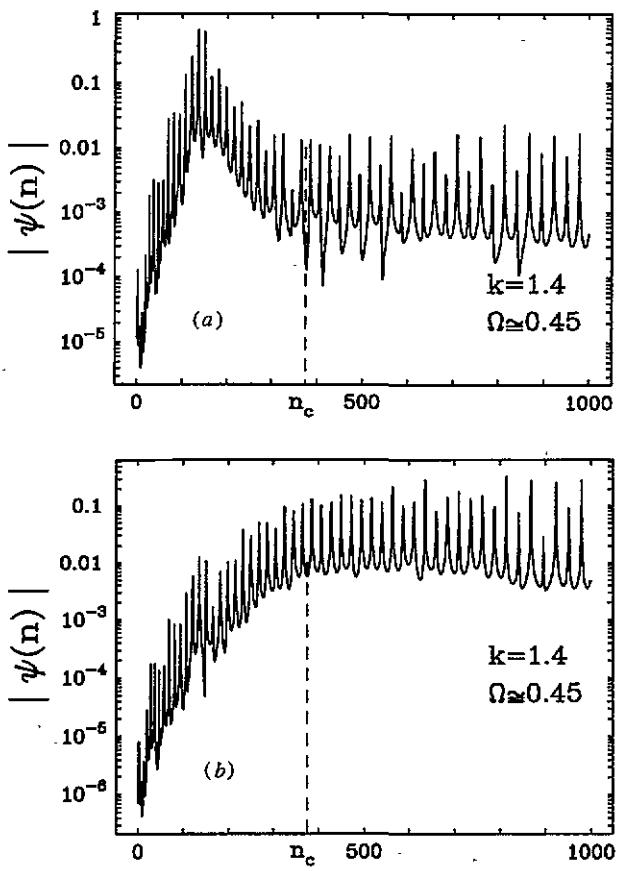

Figure 10. Two typical forms of the eigenstates of the semiclassical matrix on the large scale. The point n_c that is predicted by the theory is marked.

$$\frac{k(n\hbar)^{2/3}}{\pi\Omega\hbar} < 3\Omega(n\hbar)^{1/3}\,. \tag{4.43}$$

In contrast, if $b(n) \gg \Delta n$, there can be multiphoton transitions within the classically allowed region, transitions will occur more easily and the asymptotic power law found in the previous subsection is expected. This defines a critical value of n_c, below which the functions are expected to be localized:

$$n_c = (3\pi)^3 \frac{\Omega^6}{k^3}\hbar^2\,. \tag{4.44}$$

A numerical study of this crossover was performed in order to check the scaling law (4.44). For this purpose, approximate matrices, given by (3.28), of size up to 1200 were used. Two typical quasi-energy states of such matrices are shown in figure 10(*a*) and (*b*), with n_c marked on the figure. (Equation (4.44) gives only the scaling; a numerical prefactor is extracted from the calculations, as will be explained below.) As seen from the figure, this value is not a well defined point but rather a region of crossover. In addition, its exact location is slightly different in each quasi-energy state. In order to study its dependence on k and Ω, some averaging procedure is required. It turns out that technically the states of the kind shown in figure 10(*b*) are easier to handle numerically. For each value of the parameters k and Ω, the approximate matrix (3.28) was diagonalized numerically. All the states with an absolute value having the general form of figure 10(*b*), were picked out and smoothed around the photonic peaks. Since the positions of the peaks are different in each state, this resulted in smoothed states that are sampled each at a different set of discrete points. Therefore, in order to average over all these smoothed states, binning had to be used. The size of the bin was chosen so that a statistically significant number of sample points (several hundreds) were counted in each bin. The resulting averaged state $\overline{|\psi|}$ has a smooth crossover, of the form $\overline{|\psi(n)|} \sim 1 - e^{-\kappa n/n_c}$. From this, the point n_c can be extracted, which in general depends on κ. However, for several choices of κ which are of order unity, the scaling of n_c with the parameters k and Ω turns out to be the same. The results of these calculations are summarized in figure 11. Each point on the graph corresponds to a different

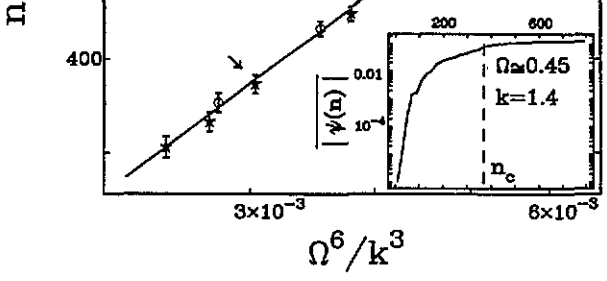

Figure 11. The scaling of n_c with k and Ω. Different values of Ω with $k = 1$ (circles); different values of k with $\Omega \approx 0.45$ (stars). $\hbar = 3\pi$ for all points. Each point was obtained by averaging the absolute value over many states, resulting in a smooth function such as that in the inset, corresponding to the point marked by an arrow.

set of values (k, Ω). The error bars result from the bin size. The inset shows an example of one of the averaged states from which a value of n_c was extracted, with $\kappa = \ln 2$. The corresponding point in the main figure is marked by an arrow. It is seen that the theoretical scaling law agrees perfectly with the numerical results. Allowing for a numeric prefactor in (4.44), this is found from the figure to be approximately 0.65.

5. Summary and discussion

In this paper, we considered the model system (1.2) as a prototype for a class of periodically driven one-dimensional systems which are inherently different from the kicked rotor, although the classical motion is chaotic. This class is characterized by the unperturbed system having a spectrum which is asymptotically a slowly varying function of the main quantum number n. It includes, among others, the bound spectrum of the hydrogen atom, and power-law potential wells with a power smaller than 2. A general method for the approximate analytical treatment of such systems was suggested and applied in detail to the system (1.2).

For the solution of the classical equations of motion, perturbation theory was used, with a small parameter ϵ which is the ratio between the unperturbed frequency and the driving frequency. This expansion becomes better at high energies. In particular, for every strength of the external driving, there exists a regime high enough in energy such that the expansion is valid. The small parameter is treated as a dynamical variable, and its time variation is related to that of the canonical action variable. The classical trajectories for one driving period are expressed in terms of a power series in ϵ. Since the driving period is a very short time scale in the problem, a semiclassical calculation of the Floquet operator is expected to be very accurate. This calculation is performed using a uniform (Bessel) approximation, taking as input the approximate classical trajectories. The resulting Floquet matrix was found to have an effectively finite bandwidth, but its width at the column n is proportional to $n^{2/3}$. To the leading order, the diagonal elements are the free-propagation factors, their phases depending on the unperturbed energy levels E_n. The off-diagonal elements are small, of the order ϵ. The characteristics of the approximate matrix, as well as its eigenstates, were compared to those of the exact matrix by numerical calculations, and good agreement between the two was found.

The increasing bandwidth structure of the propagator was found numerically for the model system (1.2), with $\cos \Omega t$ replaced by a periodic function consisting of two truncated parabolas [48]. A power of 0.5–0.7 was fitted to the bandwidth. All the calculations of the present paper are relevant for that driving as well, and a bandwidth varying as $n^{2/3}$ is predicted theoretically. For any time dependence that generally resembles a sine function, i.e. a smooth function with one positive and one negative extremum, there are two classical trajectories which coalesce, and therefore the Bessel approximation is applicable resulting in a form of the Floquet matrix similar to the one obtained here. A driving by δ-functions in time is more problematic, and a direct application of the method presented here is not possible. Indeed, in numerical calculations of the Floquet matrix for this form of driving it was found that it does not have a band structure, but rather a power-law decay, and that the eigenstates exhibit an asymptotic decay with the same power [35].

From this work the following general form of eigenstates of the evolution operator $\hat{U}$ emerges. The states are combinations of quasi-resonances that are approximately equally spaced in energy. The lineshape of all the quasi-resonances is similar, and depends only on their relative position compared to the lattice in action n. The analytic form of these quasi-resonances is given by (4.24). On the quasi-resonances is superimposed an envelope,

which is exponential for $n < n_c$ and a power law for $n \gg n_c$. The crossover value n_c, which is proportional to $(\hbar^2\Omega^6/k^3)$, is the value of n for which the bandwidth of the semiclassical matrix is of the order of the distance between quasi-resonances. In figure 10 representative eigenstates are depicted. If the maximum of the state is below n_c, the shape is similar to figure 10(a), while if it is above n_c the shape is similar to figure 10(b). For n much larger than n_c, the envelope decays with the number of quasi-resonance j as a power law, namely as $j^{-\beta}$, where β is proportional to $(\hbar\Omega^3/k^2)$ (see equation (4.42)). The power of decay as a function of n is $(2\beta/3)$. For $\beta \leqslant \frac{1}{2}$ these states are not normalizable, while for $\beta > \frac{1}{2}$ they are normalizable. This last result was also found in previous works [32, 40]. In this work, it was obtained in the framework of a model for the envelope superimposed on the quasi-resonances, which was developed by 'sewing' together solutions of a linear local approximation to the semiclassical evolution operator. Our model for the envelope (4.40) is a refined version of the model proposed by de Oliveira *et al* [32]. The present work justifies the basic assumptions of this previous work, and provides many details on the structure of the eigenstates on local scales. Because of limited computer power, we could not perform a numerical test of the asymptotic behaviour of the wavefunctions and of the long-time dynamics of the exact model. It is quite possible that the delocalization transition found in earlier numerical calculations [40] for a finite basis, results from the variation of n_c compared to the size of the basis, rather than the transition of β through its critical value. This issue should be left for further investigation.

Acknowledgments

This research was supported in part by the US–Israel Binational Science Foundation, and by the fund for promotion of research at the Technion. Part of the work was done during a workshop that was organized in Como by G Casati and G Mantica and was sponsored by the European Science Foundation. It is our great pleasure to thank O Agam, G Casati, B Eckhardt, I Guarneri, A Iomin, J Leopold, N Moiseyev, U Peskin, R E Prange, D Shepelyansky, U Smilansky and M Wilkinson for informative and inspiring discussions. Special thanks go to the referee of *J. Phys. A: Math. Gen.*, who pointed out to us an error in the first version of this paper.

Appendix A. Second-order solution for θ

In this appendix the next correction to the time dependence of θ will be calculated for completeness. This corresponds to the second order in ϵ, and takes into account the leading order time variation of the action variable.

We assume a formal expansion for $\theta(\tau)$ in the small (constant) parameter ϵ_0,

$$\theta(\tau) = \theta_0(\tau) + \theta_1(\tau)\epsilon_0 + \theta_2(\tau)\epsilon_0^2 + \cdots \tag{A.1}$$

and a similar expansion for $\epsilon(\tau)$. To second order, we substitute the solution $\epsilon(\tau)$ to the corresponding order in the equation of motion (2.11) for $\theta(\tau)$.

Consider first the case of a cycle with no collision, $\theta_0 < \theta_0^*$. In this case, we use the first two terms of (2.18) for $\epsilon(\tau)$ to write the equation for $\theta(\tau)$,

$$\dot\theta = \dot\theta_0 + \dot\theta_1\epsilon_0 + \dot\theta_2\epsilon_0^2 = \left[\epsilon_0 - \frac{k}{\pi^2}\epsilon^2(\theta_0 - \pi)\sin\tau\right] + \frac{k}{\pi^2}\left[\epsilon_0 - \frac{k}{\pi^2}\epsilon^2(\theta_0 - \pi)\sin\tau\right] \times[2\pi(\theta_0 + \theta_1\epsilon_0) - (\theta_0^2 + 2\theta_0\theta_1\epsilon_0)]\cos\tau \tag{A.2}$$

where the dot denotes derivative with respect to τ. Comparing equal powers of ϵ_0 and integrating, the solution to second order is found to be

$$\theta(\tau) = \theta_0 + \epsilon_0\tau + \frac{k}{\pi^2}\epsilon_0 a(\theta_0)\sin\tau + \frac{k}{\pi^2}\epsilon_0^2(\theta_0 - \pi[2\tau\sin\tau + 3\cos\tau - 3] - \frac{3k^2}{2\pi^4}\epsilon_0^2(\theta_0 - \pi)a(\theta_0)\sin^2\tau\,. \tag{A.3}$$

This solution consists of a linear time dependence, with oscillatory terms superimposed on it. At the end of the cycle, $\tau = 2\pi$, one has

$$\theta(2\pi) = \theta_0 + 2\pi\epsilon_0 \tag{A.4}$$

which is the same as the first-order result.

For a cycle in which a collision occurs, the two expressions, before and after the collision, must be distinguished. For the first one, $\tau < \tau*$, the equation for θ is the same as (A.2), and the solution is (A.3). It should be noticed that now the last term in (A.3) is of order ϵ_0^3, since for a cycle with a collision $a(\theta_0) = \mathcal{O}(\epsilon_0)$. After the collision, $\tau > \tau^*$, one has to substitute in the equation for $\theta(\tau)$ the corresponding expression for $\epsilon(\tau)$,

$$\epsilon(\tau) = \epsilon_0 - \epsilon_0^2\frac{k}{\pi^2}[(\theta_0 - 3\pi)\sin\tau + 2\pi\sin\tau^*] \tag{A.5}$$

and to require the explicit periodicity in $a(\theta)$ to the order ϵ_0

$$a(\theta) \approx 2\pi(\theta_0 + \theta_1\epsilon_0 - 2\pi) - ((\theta_0 - 2\pi)^2 + 2\theta_1(\theta_0 - 2\pi)\epsilon_0)\,. \tag{A.6}$$

The solution to second order is, for $\tau > \tau^*$,

$$\theta(\tau) = \theta_0 + \epsilon_0\tau + \frac{k}{\pi^2}\epsilon_0\left[\bar{a}(\theta_0)\sin\tau + b(\theta_0)\sin\tau^*\right] + \frac{k}{\pi^2}\epsilon_0^2(\theta_0 - \pi) + \frac{k}{\pi^2}\epsilon_0^2(3\pi - \theta_0)[2\tau\sin\tau + \cos\tau] - \frac{2k^2}{\pi}\epsilon_0^2\left[(\tau + \tau^*)\sin\tau^* + \cos\tau^*\right] \tag{A.7}$$

where we defined the following functions of θ_0:

$$\bar{a}(\theta_0) = 2\pi(\theta_0 - 2\pi) - (\theta_0 - 2\pi)^2 \qquad b(\theta_0) = a(\theta_0) - \bar{a}(\theta_0)\,. \tag{A.8}$$

Note that the first order term in (A.7) differs from that of (2.12) by a quantity which is of order ϵ^2. The mapping for the canonical variables I and θ can now be written, to this order of the approximation, as

$$I_{n+1} = \begin{cases} I_n & \theta_n < \theta^* \\ I_n + \dfrac{2k}{\pi\Omega}I_n^{2/3}\sin\tau^* + \dfrac{8k^2}{3\Omega^2\pi^2}I_n^{1/3}\sin^2\tau^* & \theta_n > \theta^* \end{cases} \tag{A.9}$$

$$\theta_{n+1} = \begin{cases} \theta_n + \dfrac{2\pi}{3\Omega}I_n^{-1/3} & \theta_n < \theta^* \\ \theta_n + \dfrac{2\pi}{3\Omega}I_n^{-1/3} + \dfrac{2k}{9\pi\Omega^2}I_n^{-2/3}\left[1 - (2\pi - \tau^*)\sin\tau^* - \cos\tau^*\right] & \theta_n > \theta^*\,. \end{cases}$$

Appendix B. Area preservation of the map

In this appendix, the Jacobian of the perturbative classical map is calculated to lowest order. Due to the dependence of the small parameter $\epsilon_n = \omega_0(I_n)/\Omega$ on the action variable, it is not *a priori* clear to what order the map should be calculated so that its Jacobian is correct to first order. In general, the classical mapping has the following form:

$$I_{n+1} = I_n + A(\theta_n, \tau^*) I_n^{2/3} + B(\theta_n, \tau^*) I_n^{1/3} + \cdots \tag{B.1}$$

$$\theta_{n+1} = \theta_n + C(\theta_n, \tau^*) I_n^{-1/3} + D(\theta_n, \tau^*) I_n^{-2/3} + \cdots \tag{B.2}$$

where τ^* depends on both I_n and θ_n. In order to see which terms contribute to the Jacobian to first order in ϵ_n, the partial derivatives $(\partial\tau^*/\partial I_n)$ and $(\partial\tau^*/\partial\theta_n)$ must be calculated as a power series in ϵ_n. The collision time τ^* is defined by the equation $\theta(\tau^*) = 2\pi$, or explicitly, to second order in ϵ_n,

$$2\pi = \theta_n + \epsilon_n\tau^* + \frac{k}{\pi}\epsilon_n a(\theta_n)\sin\tau^* + \frac{k}{\pi^2}\epsilon_n^2(\theta_n - \pi)[2\tau^*\sin\tau^* + 3\cos\tau^* - 3]\,. \tag{B.3}$$

Differentiating both sides of the equation with respect to θ_n yields

$$\left(\frac{\partial\tau^*}{\partial\theta_n}\right) \approx \frac{-1}{\epsilon_n} - \frac{k}{\pi^2}(\pi - \theta_n)\sin\tau^* + \frac{k\,a(\theta_n)}{\pi^2\epsilon_n}\cos\tau^* + \frac{2k}{\pi^2}(\pi - \theta_n)\tau^*\cos\tau^*\,. \tag{B.4}$$

Making a change of variables correct to first order in ϵ_n, namely $\tau^* = (2\pi - \theta_n)/\epsilon_n + \mathcal{O}(\epsilon_n)$, one finds that, in terms of the variable I,

$$\left(\frac{\partial\tau^*}{\partial\theta_n}\right) = -3\Omega I_n^{1/3} + \frac{k}{\pi}\sin\tau^* + \mathcal{O}(I_n^{-1/3})\,. \tag{B.5}$$

A similar calculation for I yields the following partial derivative:

$$\left(\frac{\partial\tau^*}{\partial I_n}\right) = \frac{\tau^*}{3}I_n^{-1} - \frac{k}{9\pi\Omega}I_n^{-4/3}\left[\tau^*\sin\tau^* + 2(\cos\tau^* - 1)\right] + \mathcal{O}(I_n^{-5/3})\,. \tag{B.6}$$

Taking into account the fact that C is constant and that A does not depend explicitly on θ_n, one concludes that the leading contributions to the Jacobian come from the first correction to I_n, namely from A, and from the two first corrections to θ_n, namely C and D. The resulting partial derivatives are

$$\begin{aligned}
\left(\frac{\partial I_{n+1}}{\partial I_n}\right) &= 1 + \frac{2k}{3\pi\Omega}I_n^{-1/3}\left[2\sin\tau^* + \tau^*\cos\tau^*\right] + \mathcal{O}(I_n^{-2/3}) \\
\left(\frac{\partial I_{n+1}}{\partial\theta_n}\right) &= -\frac{6k}{\pi}I_n\cos\tau^* - \frac{6k^2}{\pi^2\Omega}I_n^{2/3}\sin\tau^*\cos\tau^* + \mathcal{O}(I_n^{1/3}) \\
\left(\frac{\partial\theta_{n+1}}{\partial I_n}\right) &= -\frac{2\pi}{9\Omega}I_n^{-4/3} + \mathcal{O}(I_n^{-5/3}) \\
\left(\frac{\partial\theta_{n+1}}{\partial\theta_n}\right) &= 1 + \frac{2k}{3\pi\Omega}I_n^{-1/3}\left[(2\pi - \tau^*)\cos\tau^* - 2\sin\tau^*\right] + \mathcal{O}(I_n^{-2/3})
\end{aligned} \tag{B.7}$$

where in the last derivative, the expression $(2\pi - \theta_n)$ was replaced by $\epsilon_n\tau^*$, which is equivalent to the leading order. It is therefore seen that the deviation of the Jacobian from unity is of order $I_n^{-2/3}$, i.e. of order ϵ_n^2.

Appendix C. Details of the exact solution to the local eigenvalue equation

In this appendix some details of the derivation of the wavefunction (4.17) of the linear model are presented. The series in the exponent of (4.17) can be summed exactly by using the identity

$$\sum_{m=1}^{\infty} \frac{\cos(m\theta)}{m^2-\rho^2} = \frac{1}{2\rho^2} - \frac{\pi}{2\rho}\frac{\cos[\rho(\theta-\pi)]}{\sin[\rho\pi]} \qquad 0<\theta<2\pi \qquad \rho \neq \text{integer}. \tag{C.1}$$

In our case $\rho = 1/\epsilon$, and the equation can be integrated to find the sum

$$\sum_{m=1}^{\infty} \frac{\sin(m\theta)}{m(m^2-1/\epsilon^2)} = \frac{\epsilon^2}{2}(\theta-\pi) - \frac{\epsilon^2}{2}\pi\frac{\sin[(\theta-\pi)/\epsilon]}{\sin[\pi/\epsilon]}. \tag{C.2}$$

Thus the quasi-energy eigenfunction in θ is

$$\langle\theta|\psi_\lambda\rangle = \exp \mathrm{i}\left\{\mu\theta + \frac{\zeta}{2\pi}\left((\theta-\pi) - \pi\frac{\sin[(\theta-\pi)/\epsilon]}{\sin[\pi/\epsilon]}\right)\right\}. \tag{C.3}$$

Now the Fourier coefficients of this function must be calculated to get the quasi-energy states in the l-representation:

$$\langle l|\psi_\lambda\rangle = \frac{1}{2\pi}\int_0^{2\pi} \langle\theta|\psi\rangle \mathrm{e}^{-\mathrm{i}l\theta}\,\mathrm{d}\theta. \tag{C.4}$$

Defining $B = \zeta/2\sin(\pi/\epsilon)$ and using in this the expansion

$$\mathrm{e}^{-\mathrm{i}B\sin x} = \sum_{m=-\infty}^{\infty} J_m(B)\,\mathrm{e}^{-\mathrm{i}mx} \tag{C.5}$$

where J_m is the Bessel function of integer order m, one obtains the function (4.17). Notice that this function decays asymptotically as $1/l^3$ as expected, although each term in the infinite sum decays only as $1/l$.

Appendix D. Calculation of quasi-resonance widths

In this appendix the distribution of quasi-resonance widths is calculated. It will be assumed that the quasi-resonances are independent. This is justified asymptotically, although the decay of each quasi-resonance can be relatively slow, since their separation grows with n, whereas their typical decay is independent of parameters.

Using the local sinc approximation for the single resonance, (4.24), and denoting by $M=(n-n_j)$ the distance from its peak, we write

$$\frac{\sin[(M+\delta)\pi]}{(M+\delta)\pi} = \frac{(-1)^M\sin(\pi\delta)}{(M+\delta)\pi}. \tag{D.1}$$

The maximum is at $M=0$, and the relative magnitude of the function at point M is $|\delta/(M+\delta)|$. Defining the width $\Gamma(D)$ of the quasi-resonance as the number of lattice sites included in $1/D$ of its maximum value, one finds (4.31) for the width. It is seen that with no deviations, $\delta = 0$, the width is 1. For any given D, one can calculate the width as a function of δ. For example, choosing $D=4$, this function is

$$\Gamma(4) = \begin{cases} 1 & |\delta| < \frac{1}{5} \\ 2 & \frac{1}{5} \leqslant |\delta| < \frac{1}{3} \\ 3 & \frac{1}{3} \leqslant |\delta| < \frac{2}{5} \\ 4 & \frac{2}{5} \leqslant |\delta| < \frac{1}{2}. \end{cases} \tag{D.2}$$

Now using the information that the δ form a pseudorandom sequence with a uniform distribution in the interval $[-\frac{1}{2}, \frac{1}{2}]$, the resulting probability distribution for the widths is $P(1) = \frac{2}{5}$, $P(2) = \frac{4}{15}$, $P(3) = \frac{2}{15}$ and $P(4) = \frac{1}{5}$. Its average is 2.133 and its variance is 1.32 (cf figure 7).

References

[1] Casati G, Guarneri I and Smilansky U (ed) 1993 *Quantum Chaos, Proc. Int. School of Physics 'Enrico Fermi' (Varenna 1991)* (New York: North-Holland)
[2] Haake F 1991 *Quantum Chaos* (New York: Springer)
[3] Casati G, Chirikov B V, Shepelyansky D L and Guarneri I 1987 *Phys. Rep.* **154** 77 and references therein
[4] Casati G, Chirikov B V, Izrailev F M and Ford J 1979 *Stochastic Behaviour in Classical and Quantum Hamiltonian Systems* (Berlin: Springer)
[5] Fishman S 1989 *Phys. Scr.* **40** 416
[6] Fishman S, Grempel D R and Prange R E 1982 *Phys. Rev. Lett.* **49** 509
Grempel D R, Prange R E and Fishman S 1984 *Phys. Rev.* A **29** 1639
[7] Giannoni M J, Voros A and Zinn-Justin J (ed) 1991 *Chaos and Quantum Physics, Proc. Les-Houches Summer School, Session LII 1989* (Amsterdam: North-Holland)
[8] Gutzwiller M C 1990 *Chaos in Classical and Quantum Mechanics* (New York: Springer)
[9] Blümel R, Fishman S and Smilansky U 1986 *J. Chem. Phys.* **84** 2604
[10] Prange R E and Fishman S 1989 *Phys. Rev. Lett.* **63** 704
[11] Agam O, Fishman S and Prange R E 1992 *Phys. Rev.* A **45** 6773
[12] Casati G and Molinari L 1989 *Prog. Theor. Phys. Supp.* **98** 287
[13] Zeldovich Y B 1967 *Sov. Phys.–JETP* **24** 1006
[14] Chirikov B V 1979 *Phys. Rep.* **52** 263
[15] Lichtenberg A J and Lieberman M A 1983 *Regular and Stochastic Motion* (Berlin: Springer)
[16] Cohen A and Fishman S 1988 *Int. J. Mod. Phys.* B **2** 103
[17] Ishii K 1973 *Prog. Theor. Phys. Suppl.* **53** 77 and references therein
[18] For a review see Fishman S Quantum localization, in [1] and references therein
[19] Shepelyansky D L 1983 *Physica* **8D** 208
[20] Casati G, Guarneri I and Shepelyansky D L 1989 *Phys. Rev. Lett.* **62** 345
[21] Fishman S, Prange R E and Griniasty M 1989 *Phys. Rev.* A **39** 1628
[22] Dittrich T and Smilansky U 1991 *Nonlinearity* **4** 59, 85
[23] Doron E and Fishman S 1988 *Phys. Rev. Lett.* **60** 867
[24] Casati G, Guarneri I and Shepelyansky D L 1988 *IEEE J. Quantum Electron.* **QE-24** 1240
[25] Jensen R V, Leopold J G and Richards D R 1988 *J. Phys. B: At. Mol. Opt. Phys.* **21** L527
[26] Blümel R and Smilansky U 1987 *Z. Phys.* D **6** 83
[27] Das-Sarma S, He S and Xie X C 1988 *Phys. Rev. Lett* **61** 2144; 1990 *Phys. Rev.* B **41** 5544
[28] Brenner N and Fishman S 1992 *Nonlinearity* **4** 211
[29] Griniasty M and Fishman S 1988 *Phys. Rev. Lett.* **60** 1334
[30] Thouless D J 1988 *Phys. Rev. Lett.* **61** 2141
[31] Izrailev F M and Shepelyansky D L 1980 *Teor. Math. Fiz.* **43** 417 (Engl. transl. 1980 *Theor. Math. Phys.* **43** 553)
[32] de Oliveira C R, Guarneri I and Casati G 1994 *Europhys. Lett.* **27** 187
[33] Richards D, Leopold J G and Jensen R V 1989 *J. Phys. B: At. Mol. Opt. Phys.* **22** 417
[34] Grempel D R, Fishman S and Prange R E 1982 *Phys. Rev. Lett.* **49** 833
Prange R E, Grempel D R and Fishman S 1984 *Phys. Rev.* B **29** 6500
[35] Shimshoni E and Smilansky U 1987 *Nonlinearity* **1** 435
[36] Fetter A L 1976 *The Physics of Liquid and Solid Helium* ed K H Bennermann and J B Ketterson (New York: Wiley)
[37] Prange R E and Nee T W 1968 *Phys. Rev.* **168** 779
[38] Koch J F and Kip A F 1965 *Low Temperature Physics (Proc. LT9)* (New York: Plenum) p 818
[39] Pustylnikov L D 1978 *Trans. Moscow Math. Soc.* **2** 1
[40] Benvenuto F, Casati G, Guarneri I and Shepelyansky D L 1991 *Z. Phys.* B **24** 159
[41] Deylon F, Simon B and Soulliard B 1984 *Phys. Rev. Lett.* **52** 2187; 1985 *Inst. H Poincaré* **42** 283
[42] Miller W H 1974 *Adv. Chem. Phys.* **25** 69
[43] Chester C, Friedman B and Ursell F 1957 *Proc. Camb. Phys. Soc.* **53** 599

[44] Levit S and Smilansky U 1977 *Ann. Phys, NY* **103** 198; **108** 165
[45] Berry M V and Mount K E 1972 *Rep. Prog. Phys.* **35** 315
[46] Stine J R and Marcus R A 1973 *J. Chem Phys.* **59** 5145
Connor J N L and Mayne H R 1978 *Mol. Phys.* **37** 1
[47] Watson G N 1958 *A Treatise on the Theory of Bessel Functions* 2nd edn (Cambridge: Cambridge University Press)
[48] Dembinski S T, Makowski A J and Peplowski P 1993 *Phys. Rev. Lett.* **70** 1093
[49] Peskin U and Moiseyev N 1993 *J. Chem. Phys.* A **99** 4590
[50] Sambe H 1973 *Phys. Rev.* A **7** 2203